Titre: Title:	Optimization of the Rate and Level of Porosity Generation in Electrode Films for Application in Batteries
Auteur: Author:	Zohreh Mosaferi
Date:	2018
Type:	Mémoire ou thèse / Dissertation or Thesis
Référence: Citation:	Mosaferi, Z. (2018). Optimization of the Rate and Level of Porosity Generation in Electrode Films for Application in Batteries [Mémoire de maîtrise, École Polytechnique de Montréal]. PolyPublie. https://publications.polymtl.ca/3041/

URL de PolyPublie: PolyPublie URL:	https://publications.polymtl.ca/3041/
Directeurs de recherche: Advisors:	Abdellah Ajji
Programme: Program:	Génie chimique

UNIVERSITÉ DE MONTRÉAL

OPTIMIZATION OF THE RATE AND LEVEL OF POROSITY GENERATION IN ELECTRODE FILMS FOR APPLICATION IN BATTERIES

ZOHREH MOSAFERI

DÉPARTEMENT DE GÉNIE CHIMIQUE

ÉCOLE POLYTECHNIQUE DE MONTRÉAL

MÉMOIRE PRÉSENTÉ EN VUE DE L'OBTENTION

DU DIPLÔME DE MAÎTRISE ÈS SCIENCES APPLIQUÉES

(GÉNIE CHIMIQUE)

AVRIL 2018

UNIVERSITÉ DE MONTRÉAL

ÉCOLE POLYTECHNIQUE DE MONTRÉAL

Ce mémoire intitulé :

OPTIMIZATION OF THE RATE AND LEVEL OF POROSITY GENERATION IN ELECTRODE FILMS FOR APPLICATION IN BATTERIES

présenté par: MOSAFERI Zohreh

en vue de l'obtention du diplôme de: Maîtrise ès sciences appliquées

a été dûment accepté par le jury d'examen constitué de :

M. DUBOIS Charles, Ph. D., président

M. AJJI Abdellah, Ph. D., membre et directeur de recherche

M. PREBE Arnaud, Ph. D., membre externe

DEDICATION

To my beloved husband, Yousef.

ACKNOWLEDGEMENTS

Firstly, I would like to express my gratitude to my supervisor, Prof. Abdellah Ajji, for his continuous support and guidance through my Masters' research. I am also thankful to Dr. Arnaud Prébé for his help, suggestions and feedbacks to this work.

I would like to thank all the technical and administrative staffs of Chemical Engineering Department of Ecole Polytechnique de Montreal and Hutchinson Co. for their kind cooperation during this project, specially Ms. Claire Cerclé and Mr. Mattheiu Gauthier.

In undertaking this work, I had the honor to collaborate with the other student in Prof. Ajji's group. I would like to specially thank my friend Ms. Zahra Kordjazi, who supported me greatly during the past two years. I would also like to thank Ms. Fatma Ben Dheib who did a favor to translate my abstract to French.

This work could not be completed without the unconditional love of my parents, Mohammad Jafar Mosaferi and Masoomeh Mosaferi. Although they were far from me in the past three years, they have always supported me and encouraged me to take steps forward in my education.

Lastly, my deepest gratitude goes to my husband, Yousef Saatchi Tabriz. His continued and unfailing love, patience and encouragement during my pursuit to master's degree, made finishing this work possible for me.

RÉSUMÉ

Dans le but de générer de la porosité dans les électrodes poreuses des batteries Li-ion, le carbonate de propylène (PPC) a été utilisé comme phase sacrificielle. 3 catalyseurs (un générateur photo acide, un générateur d'acide thermique et un peroxyde) ont été rajoutés en faible fraction en masse à cette phase pour augmenter la vitesse de dégradation et leurs effets ont par la suite été étudiés. L'analyse thermogravimétrique (ATG) a montré que ces catalyseurs ne réduisent pas la température de décomposition du PPC.

Des composés contenant un liant, une phase sacrificielle et des ingrédients actifs ont alors été préparés par mélange à chaud et calandrés ensuite pour atteindre une épaisseur spécifique. Ces films ont été exposés à la radiation infra-rouge pour y générer de la porosité. Trois lampes infra-rouges avec différentes longueurs d'onde ont été testées et la lampe choisie est celle avec laquelle le plus haut taux de dégradation du PPC a été obtenue. Pour l'étape suivante, le temps et la température de dégradation ont été optimisés pour chaque échantillon. Les résultats obtenus ont montré que la lampe ayant la plage de longueurs d'onde la plus longue augmente le taux de décomposition du PPC et qu'il faut moins de temps pour la génération de la porosité.

Un fois cette partie complétée, la porosité des films d'électrode a été étudiée par microscopie électronique à balayage (MEB), porosimétrie par intrusion de mercure (PIM) et par la méthode de saturation du solvant. Les résultats de la MEB ont montré que la taille des pores dans les composés ayant le graphite comme ingrédient actif est plus importante que celle des autres composés avec des ingrédients actifs différents.

La comparaison des résultats obtenus par la MEB et la PIM a montré que la caractérisation par MEB sous-estime la taille des pores et la porosité totale. La porosité totale a été déterminée également par la méthode de saturation du solvant et les résultats ont concordés avec ceux de la PIM.

ABSTRACT

For porosity generation in porous electrodes of Li-ion batteries, polypropylene carbonate (PPC) as a sacrificial phase was used. To increase degradation rate of the sacrificial phase, 3 catalysts (a photo acid generator, a thermal acid generator and a peroxide) in low weight fractions, were separately added to the PPC and their effect was studied. Thermogravimetric analysis (TGA) tests showed that none of these catalysts could decrease the decomposition temperature of PPC.

Then, a compound containing a binder, a sacrificial phase and active ingredients was prepared by hot mixing. After mixing, the final compounds were calendered to reach a specific thickness. These films were exposed to infrared radiation to generate porosity in it. 3 infrared lamps with different wavelength ranges were initially used and one of them, for which the highest degradation rate of PPC was obtained, was chosen. In the next step, time and temperature of degradation for each sample was optimized for that wavelength. The results showed that the lamp with the longest wavelength range, increases the decomposition rate of PPC and less time is needed for porosity generation.

After this part was completed, porosity of electrode films was studied using scanning electron microscopy (SEM), mercury intrusion porosimetry (MIP) and solvent saturation method. The results of SEM showed that the pore size in the compounds containing graphite as active ingredient is larger than other compounds with other active ingredients.

Comparing SEM and MIP results showed that SEM underestimates the pore size and total porosity. By solvent saturation method, the total porosity was calculated and was in agreement with MIP results.

TABLE OF CONTENTS

LIST OF TABLES

LIST OF FIGURES

LIST OF SYMBOLS AND ABBREVIATIONS

MEB	Microscopie électronique à balayage
PIM	Porosimétrie par intrusion de mercure
ATG	Analyse thermogravimétrique
PPC	Polypropylene carbonate
PPCL	Liquid Polypropylene carbonate
HNBR	Hydrogenated nitrile butadiene rubber
EPDM	Ethylene propylene diene monomer rubber
TPE	Thermoplastic elastomer
Li-ion	Lithium ion
PAG	Photo acid generator
TAG	Thermal acid generator
TGA	Thermogravimetric analysis
MEB	Microscopie électronique à balayage
SEM	Scanning electron microscopy
MIP	Mercury intrusion porosimetry
CNT	Carbon nanotube
PDMS	Poly(dimethylsiloxane)
PMMA	Poly (methyl methacrylate)
HNBR	Hydrogenated nitrile butadiene rubber
EPDM	Ethylene propylene diene monomer rubber
TPE	Thermoplastic elstomer
IR	Infrared

FTIR	Fourier Transform Infrared
UV	Ultraviolet
UV-VIS-NIR	Ultraviolet visible near infrared
LFP	Lithium iron phosphate
LTO	Lithium titanate
CLTO	Carbon coated lithium titanate
ΔP	Pressure difference
r_1, r_2	Geometric parameters of pores
μm	Microns
min	Minute
τ_{eq}	Characteristic diffusion time
D	Diffusion coefficient
L	Characteristic diffusion length
Nm	Nanometer

CHAPTER 1 INTRODUCTION

Growing use of renewable energies in transport applications and communication made rechargeable lithium ion batteries in very high demand [1]. The main chemical reaction in these batteries is called charge/discharge reaction and consists in intercalation/deintercalation of Li-ion on the electrodes and it is a reversible process [2, 3]. In the applications such as electric vehicles, shorter recharging times are needed in order to grow the market [4]. Although Li-ion batteries have very high energy densities, their diffusion rate is very low. By enhancing the structure of the electrodes, this problem can be solved. Shorter diffusion length in the electrodes will make their characteristic diffusion time shorter. To achieve a high diffusion rate Li-ion battery, porous electrodes, with large contact area, can be used [5-7]. The porous compounds as electrodes have a continuous structure of pores and active fillers and can significantly reduce the diffusion time [4]. Several studies have been made to make porous electrode materials [8]. The first method is the extraction of one phase from the compound [8, 9]. The problem associated with this method is the usage of organic solvent to dissolve the components. In fact, these organic solvents are hazardous to environment, toxic and flammable. Porosity control in this method during solvent evaporation is difficult and it puts a limit for active fillers[10].

Hard templating is also offered to produce porous electrodes. A thermosetting resin combined with active fillers is injected to a mold and baked. The major drawback of this method is the non-transformability of the electrode after baking and high baking times needed for precursor resin [4, 7, 11].

Hutchinson company offered melt mixing of the ingredients with a sacrificial phase available in the compound and thermal decomposition of sacrificial phase after compounding. This method does not need using any solvent and has lower environmental risks [7, 10].

The problem associated with this technique is the high energy and time that is needed for decomposition of sacrificial phase. The proposed material for sacrificial phase is polypropylene carbonate for its low degradation temperature. The electrodes with thicknesses of about 50 μm to 200 μm need to stay in a conventional oven about 20 to 45 min at 230°C to 240°C. The

decomposition temperature and time depend on the final composition and the active fillers used in the compound [10].

The main objective of this study is to reduce degradation time of polypropylene carbonate (PPC) that is used as sacrificial phase in the process of producing porous electrode and quantifying porosity in the electrode.

In this study, a literature review is first presented in Chapter 2 on Li-ion batteries structure, different methods of porosity generation in electrodes, degradation behavior of PPC and porosity measurement techniques. Then, the experimental work, results, discussion and conclusions are presented in the following chapters.

The first part of the experimental work was to study the PPC degradation behavior under different environments and combined with different catalysts using thermogravimetric analysis (TGA). Then, compounds of binders, active fillers and sacrificial phase were prepared by melt mixing to see the effect of each active fillers on the decomposition of PPC and also perform degradation studies under infrared lamps to study its effectiveness on decomposition time. At the end of this work, porosity measurements were performed using imaging techniques, mercury intrusion porosimetry and liquid saturation technique.

1.1 Problem Identification and Originality

As it was briefly discussed in the previous part, porosity generation in electrodes could cause environmental damage and safety issues. To reduce these problems, which are caused mostly by solvent in the porosity generation, Hutchinson Co. offered using thermal degradation of a sacrificial phase for porosity generation [7]. In their method, conventional ovens are used, which need high levels of temperature and energy. The degradation of PPC in these ovens is also very time consuming. High energy and duration of degradation makes the cost of this process high. To reduce the costs and energy use in this method, lowering the degradation temperature of PPC as sacrificial phase and using other techniques for heat application to the electrodes are desired.

The originality of this study is the optimization of time and temperature in which degradation of sacrificial phase is completed. In this study, the effect of using infrared lamps, as the heating media, instead of conventional ovens for PPC decomposition is studied. On the other part, the effect of

three different catalysts on the degradation behavior of PPC is studied to see whether they can reduce degradation temperature of PPC.

1.2 Objectives

1.2.1 GENERAL OBJECTIVE

This study is aimed to accelerate the porosity generation rate in electrodes for Li-ion batteries by optimizing time and temperature in which degradation of a sacrificial phase occurs.

1.2.2 SPECIFIC OBJECTIVES

- Addition of several catalysts separately to the sacrificial phase to study their effectiveness on lowering degradation temperature. If they were effective, they will be added in the final compound formulation.
- Degradation of electrodes under infrared lamps with varying time and temperature to choose the optimum point. Infrared lamps with different wavelength range will be tried.
- Porosity measurement of final porous electrodes using different laboratory techniques.

1.3 Dissertation Plan

In Chapter 2, a literature review is presented. Starting with Li-ion batteries and its elements and continuing with the properties of porous electrodes. After studying benefits of porous electrodes, different methods are reviewed for porosity generation. The method that is going to be discussed is introduced and at the end, theories of porosity measurements are also reviewed.

In Chapter 3, materials, methods and experiments that were used in this work are introduced. Results of the tests are presented and discussed in Chapter 4 and the final conclusion with the recommendation for future works are presented in Chapter 5.

CHAPTER 2 LITERATURE REVIEW

2.1 Lithium ion batteries

Rechargeable Lithium ion battery is the leading energy storage device with applications in communication devices such as cell phones and tablets, transport and renewable energy sources[1]. The major advantage of this type of batteries is their high energy density and cycling performance. It was first produced by Asahi co. in Japan and commercialized by Sony in 1991. The benefits of Li-Ion batteries such as high energy-density, no memory effect (as opposed to Nickel cadmium (Ni-Cd) or nickel-hydride (Ni–MH) batteries), high efficiency and long life made it acceptable rapidly[12, 13].

Batteries in general consist of one or several electrochemical cells which provide power to electronic devices. In their structure, electrolyte may be in the form of a liquid or solid. For gas or liquid electrodes, solid electrolytes are used. However, they can also be used with solid electrodes too, but the interface between two solids may cause some problems unless the electrolyte is made of polymers or electrodes are thin. In the case of liquid electrolytes, solid electrodes are prevented from contact with a separator which is electrolyte permeable. The role of electrolyte is to transfer ions form one electrode to another and to make a reversible circuit of ions [2]. In the charging process, Li ions are deintercalated from cathode and are inserted on anode layers. Decharging process is the reverse of charging reaction[3].

Two electrodes, anode and cathode, and a separator called the electrolyte are the constituents of an electrochemical cell. The electrodes are made of active particles, generally with a layered structure, in micron scale and a binder which keep them together. Usually a conductive component is also needed for having a higher electrical conductivity[4]. Electrical energy in batteries is developed by conversion of chemical energy in redox reactions between two electrodes. In this reaction, anode will be oxidized and cathode will be reduced. Since lower redox potential reaction occurs in anode in comparison to cathode, anode is considered as negative pole and cathode as positive one [14]. The exchange of Li ion during charging and discharging between two electrodes is called intercalation. This process is also called inserting a guest into a layered host. In the case of Li-ion batteries, Li-ion is the guest and electrodes are the hosts [15]. The generated voltage in Li-ion battery depends on the difference of active particles' potential in in cathode and anode and

it value can vary and go up to 3.8V. Using materials with higher potential will result in higher voltage in the battery [12]. Figure 2-1 shows the charge-discharge process in Li-ion batteries.

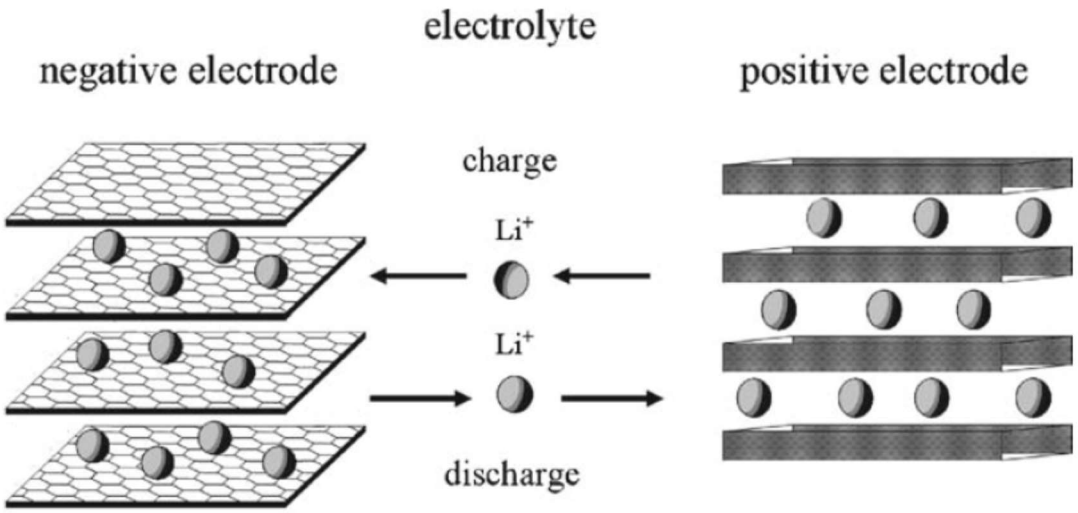

Figure 2-1. Charge/discharge process in Li ion battery with layered structured electrodes [12]

In the positive electrode of Li-ion batteries, compounds for intercalation are used in the form of $Li_xM_yX_z$, in which X can be oxygen or a polyanionic compound or complex[10]. To obtain an acceptable output voltage, a metal ion (M_y) with a high redox potential should be chosen. In the intercalation compound, a large number of Li ions should have the ability to reversibly intercalate and deintercalated. Therefore, higher value of $_x$ is required. In this process, no change in the structure of compounds should occur. Chemical stability to avoid reaction with electrolyte is an important characteristic for intercalation compound. To have a decent charge/discharge rate, high diffusion coefficient of Li ion in cathode is expected [15].

In the negative electrode, or anode, most investigated materials are graphitic and amorphous carbon materials for their high reversible capacity and low cost [16]. Contrary to cathode, anode materials should have a low redox potential for inserting Li ions into them [15].

2.2 Porous electrode structure

Growing use in applications such as electric vehicles or plug-in hybrid electric vehicles requires electrical storage devices with higher specific capacities and faster rate performance [5]. In these applications, by having a shorter time for recharging vehicles, consumers would more easily accept the usage of these technologies. Also, in renewable energy resources, wind and solar energy for

instance which are seasonal, energy densities and rate of performance should be improved for having higher charge storing [4].

One way to make the high-power requirements possible is to use capacitors and supercapacitors. In comparison to batteries, they are able to take up charge at a more rapid rate. Although, in capacitors, charge storage only occurs on the electrode surface, which allows rapid charging but low energy density. In batteries, charge storage is in the bulk, therefore supplying higher energy density. Downside of using batteries is their rate of charge delivery, which is bound by diffusion of Li ion through the bulk. To fix the low diffusion rate in batteries, the electrodes' structures are improved. Lithium ions have a characteristic diffusion time (τ_{eq}) to pass through the electrodes, which is related to the square of characteristic diffusion length ($\tau_{eq} \sim l^2/D$). D in this equation is the diffusion coefficient [5, 6]. To have a shorter diffusion time, either diffusion coefficient by improving Li ion conductor should be increased or diffusion length should be shortened. To prevent any chemical changes in the structure, the second route is preferred. Furthermore, diffusion length has a greater effect on the diffusion time for its square relationship. Therefore, it is an attractive research area in recent years [5-7]. A practical way for obtaining short diffusion time is to use porous materials for electrodes. These materials provide a wide range of advantages. First, they offer a larger contact area and a better access to electrolytes, which makes charge transfer easier. On the other hand, active fillers' walls enclosing pores could be very thin and reduce the required diffusion length. A continuous structure between pores and fillers can be reached, which can reduce diffusion time. Furthermore, a porous composite with an added conductive phase can be made to enhance conductivity of the active phase.

Classification of porous materials could be based on their pore sizes, which is in 3 classes. First, micropores which are less than 2 nm, then mesopores that have a size between 2-50 nm and macropores that are bigger than 50 nm. Other methods of classification are based on their synthesis procedure (templating and non-templating) and type of porosity which can be "textural" (voids generated between the particles) and "true" or "integral" which is the type of pore that is an integral part of a solid. In textural porosity, pore size is related to particle size, whereas is integral porosity particle size has no effect of pore size [4].

Conventional electrodes, which are made by drying or casting a slurry consist of binder, active material and conductive particles, usually have textural porosity [4]. Intensive research has been

made on making porous electrode materials by extracting one phase. In a research made by H. Lee et. Al. [8], polydimethylsiloxane (PDMS)/carbon nanotube (CNT) porous composite was made through the following procedure. First PDMS with polymethylmethacrylate (PMMA) and PDMS-b-PMMA were dissolved in toluene at 75°C. After complete dissolution, toluene was removed and CNT was mixed with the solution. Since CNT prefers mixing with PDMS, by extracting PMMA with acetic acid, porous structure will be achieved [8]. In another study, a dry mixture of lithium nickel manganese cobalt oxide as active ingredient and carbon black as conducting agent, were mixed with a polyvinylidene difluoride binder dissolved in N-methyl-2-pyrrolidone. The slurries were applied on an aluminum foil and then dried at 80°C and 120°C, each for 5 min [9]. This experiment was performed to see the effect of dry-mixing of powders before preparing the electrode.

In each of the above-mentioned experiments, an organic solvent was used to dissolve the components. For porosity generation, a drying step is included in their process. This type of process has many drawbacks such as environmental hazard and safety issues due to usage of organic solvents, as they can be toxic and flammable [7]. On the other hand, porosity control during drying of solvent can be problematic and in general, each solvent has a limit for additives in formulation.

Another method of templating electrodes is hard templating, which can be used for solid porous electrodes, anodic aluminum oxide and assemblies of colloidal particles such as silica-based or polymer-based colloidal crystals. In this method, large amount of active material combined with a precursor thermosetting resin, is injected to a mold and is baked [4, 7, 11]. The problem with this method is the non-transformability of electrode after the resin is baked and the long time that is needed for baking reaction of resin and forming crosslinks in the material. On the other hand, viscosity of the precursor resin is an essential factor in the flow of the paste through the inter-grain porosity. Therefore, high molecular weight resins, due to their low flowability and high viscosity, cannot be used in this method [10].

It is also possible to make magnetic compounds by continuous melt processing such as extrusion or internal mixing, which are used for thermoplastic polymers. The amount of active filler which can be reached greatly depends on its type. In these types of processes, high viscosity and abrasion of binder by inorganic filler is inevitable. In this method, only highly dense materials without any control on porosity can be made. To increase compatibility of active fillers with the binder, fillers'

surface should be functionalized. This step will greatly increase the cost of the process and is the its most considerable disadvantage.

Hutchinson Co. offered a new method in their invention that avoids using solvents both for its environmental hazards and also low limits for active fillers as well as making the use of active fillers without the need to add functionality possible [7]. They proposed using melt mixing of all ingredients with keeping sacrificial phase weight fraction higher than 15%. This way, viscosity and fluidity of it can be controlled. The resulting high filler polymeric compound has magnetic properties which makes it suitable for electrodes of Li-ion or sodium ion batteries and supercapacitors. Porosity of this compound, based on its application, can be controlled.[10].

This melt-mixing process has different steps. First, binder, active material and sacrificial phase are hot-mixed. In this step, the sacrificial phase content should be in the range of 20-80 wt%. Active filler content can go up to 80 wt% or 60 vol%. The high amount of active filler, allows having very high content of filler after removing sacrificial phase, without any need for surface modification or coupling agent. Porosity of the compound, size and morphology of the pores can be controlled by changing the sacrificial phase content. The melt-mixing process can be performed in an internal mixer or extruder. The obtained morphology is a co-continuous morphology of binder phase in sacrificial phase. By thermal decomposition of sacrificial polymeric phase, it can be easily extracted without having any effect on other components. If sacrificial polymer is compatible with the final application, decomposition could be carried out partially, otherwise full decomposition of sacrificial phase is expected. Thermal decomposition temperature of sacrificial phase should be at least 20℃ less than binder. To accelerate decomposition of sacrificial phase, catalysts such as photo acid generators could be used [10, 17]. Thermal decomposition could be carried out in conventional ovens or under infrared emitters. In this study, only IR emitters are going to be studied. In the next session, the materials that can be used in this process are thoroughly discussed.

2.3 Materials used in porous electrodes made by sacrificial agent decomposition

2.3.1 Active fillers

Essentially, all inorganic active fillers with the characteristics mentioned in section2.1 can be used in the structure of electrodes. $LiFePO_4$ (LFP), $Li_4Ti_5O_{12}$ (LTO), carbonated LTO, $LiCoO_2$,

$LiMnO_4$, or $LiNi_{1/3}Mn_{1/3}Co_{1/3}O_4$ could be used in cathodes and graphite or any porous carbon fillers could be used in anodes [10]. Electroconductive fillers such as carbon black, graphene, carbon nanotubes or nanofillers could be added making the whole system conductive [10]. Some of the abovementioned fillers are discussed here.

LFP is one of the important active fillers used in Li-ion batteries [10, 18-20]. It is a filler with low-cost, low-toxicity and high capacity. Its only drawback is low electrical conductivity that can be resolved with carbon-coating [18, 21], metal doping [22] and particle size reduction [23]. Its capacity is 160 mAh/g [12]. It has a very low Li ion diffusivity and electrical conductivity at room temperature (10^{-9} S/cm at room temperature) but strong stability up to 400°C [24].

LTO and carbon coated LTO are two choices for an active filler suitable for anode in Li-ion batteries[25-28]. LTO is a thermodynamically stable compound with low cost that can generate 1.5 V in the battery. Low ion diffusivity and low electrical conductivity of this powder is the disadvantages it has, which carbon-coating LTO, the problems of its low conductivity can be solved and CLTO will be produced [27].

Graphite is a layered compound, in which lithium intercalation can occur and is considered as anode material for Li ion batteries [29]. It is usually defined by a pile of carbon sheet, with the bonds of carbon which are hexagonally shaped and the sheets are connecting with Van der Waals forces. The bonds between each two carbons, with shared sp^2 hybridized bond, in the same sheet is much stronger than the bonds between two sheets. This difference in the forces makes graphite structure appropriate for Li ion to locatebetween the sheets. The storage capacity of Li ions in graphite is 372 mAh/gr [30]. It is the main material which is used for anodes in li-ion batteries for its low cost, possibility of modification and good potential [31]. Very low potential of lithium insertion on graphite anode, makes reduction of all the other active ingredients with the ability of reverse Li intercalation with graphite possible [32]. Additionally, the expansion of graphite, while Li ion is inserted on it, is very low and is the reason that the charge capacity of graphite is not affected by charge-discharge cycles [30]. The major advantage of graphite is its efficiency during repeating cycles and its drawback is its relatively low storage capacity [30].

Some metals such as Aluminum or Antimony have very high lithium storage capacity. The storage mechanism of these compounds is different from graphite and is by forming alloys with lithium. This makes their capacity much higher than graphite (993 mAh/gr for LiAl and 536 mAh for

Li_3Sb), since for insertion of Li ion in graphite 6 carbon atoms are needed but, for instance, one Aluminum atom can bond with 2-4 Li atoms. Although, this mechanism is the reason for higher expansion of alloys in comparison to graphite and can make anode structure to collapse [30, 33, 34]. This process is known as pulverization and is the primary reason for not using metal alloys as an anode in Li ion batteries, considering its fading capacity during several charge-discharge cycles [30].

Carbon nanotubes are a good candidate for anode in lithium anode batteries as a result of their exceptional tubular structure, very high conductivity and good mechanical properties [30, 35-37]. The storage capacity of CNT can go up to 600 mAh/gr which is much higher than graphite. Also, some chemical treatments can be done on CNT that can increase their capacity up to 1000 mAh/gr. In contrast with Li-metal alloys, higher capacity in CNT would not make pulverization in them. By compounding them with metal compounds, even higher capacities could be reached [30, 38]. The main drawback of CNT is that in the first charging cycle, some lithium ions are irreversibly inserted on the walls of CNT. This process makes their capacity fading through several cycles [30].

2.3.2 Binder

To keep the composition cohesive after melt process, a polymeric binder should be added.Binder or matrix phase should be one or more crosslinked or non-crosslinked elastomer with the weight fraction between 1% and 12%. The preferred binders are from the group of hydrogenated butadiene/acrylonitrile rubber, ethylene/acrylate copolymers, polyisoprenes and the mixtures of these materials. Thermoplastic elastomers are the other option for binder. The most important characteristic of the binder is to keep its elastic properties in the range of -20℃ to 80℃. Additives for crosslinking of the binder, such as peroxide catalysts, could be added [10].

2.3.3 Sacrificial phase

The polymers suggested to be used as a sacrificial phase can be in the group of polyalkene carbonates and most possibly polypropylene carbonates or polyethylene carbonates. In the case of this research, two grades of polypropylene carbonates were used [10]. Polycarbonate and specifically polypropylene carbonates are a group of polymers with low degradation temperature, which makes them appropriate for playing sacrificial phase role in various compounds and

applications. Beside from their application in porous electrodes, polypropylene carbonates can be used in manufacturing microelectromechanical applications and microfluids [17, 39].

2.3.3.1 Thermal degradation of polypropylene carbonate

Full degradation of polypropylene carbonate occurs between 200℃ and 300℃ [39]. The degradation mechanism of polypropylene carbonate greatly depends on its environment. In the inert environments, decomposition starts by chain unzipping into cyclic propylene carbonate at around 180℃ and continues by random chain scission at higher temperature of about 250℃. Chain unzipping is the process in which active chain ends, resulted by thermal energy, attack a carbon site in the backbone of the polymer and start degradation. The main product of chain unzipping is cyclic propylene carbonate. Chain scission activation energy is much higher that chain unzipping and it is not affected by chain ends. In this reaction, very high thermal energy randomly splits a C-O bond from the backbone and produces carbon dioxide and acetone [40]. In addition, the mechanism of decomposition depends on decomposition atmosphere, polymer molecular weight, ether linkages available in the backbone, and backbone regiostructure [17]. Figure 2-2 shows the mechanism of chain unzipping and chain scission.

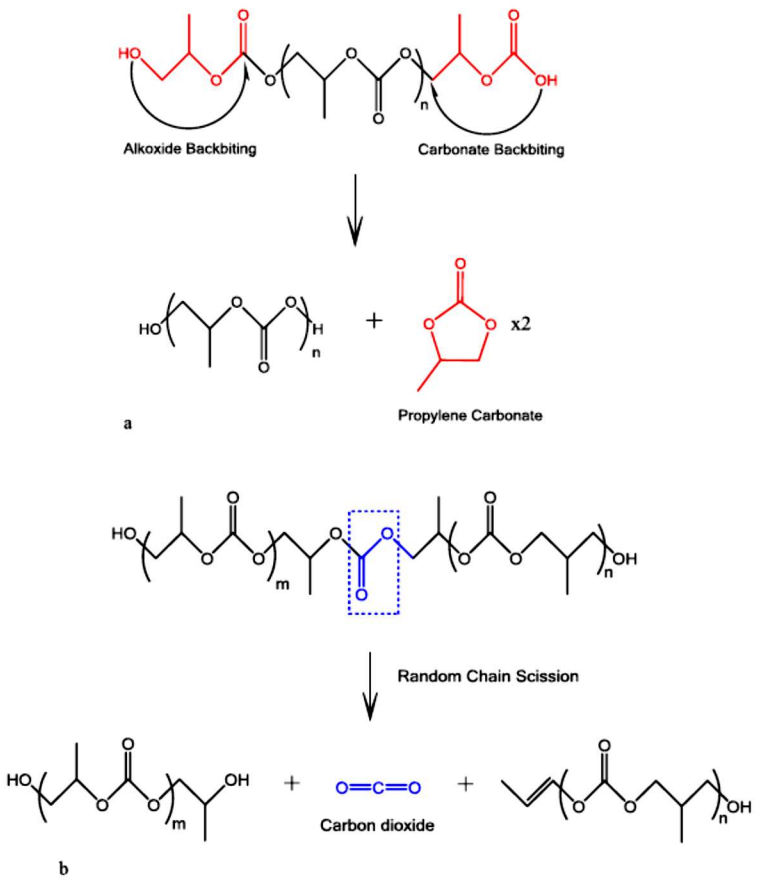

Figure 2-2. (a) Chain unzipping reaction in PPC occurring via an alkoxide or carbonate backbiting pathway creating the cyclic propylene carbonate as the product. (b) Chain scission reaction in PPC via thermally induced cleavage of CO bonds creating carbon dioxide as one of the products. [40]

Polypropylene carbonate is usually produced by copolymerization of propylene carbonate and carbon dioxide at high pressures with a catalyst. The main component of the backbone is propylene carbonate. The molecular weight of this product can go up to 10^5 g/mol [17, 41]. There might be ether linkages available in the backbone which are unwanted by-products in the polymerization. The concentration of ether links is usually less than 10 mol percent. Figure *2-3* shows the backbone structure of a typical polypropylene carbonate chain.

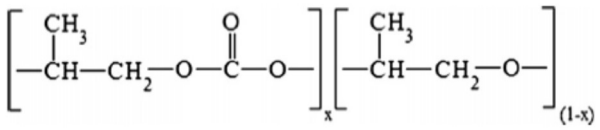

Figure 2-3. Typical structure of polypropylene carbonate, adapted from [17]

Based on the catalyst used and polymerization conditions, the backbone structure might change and this greatly influence thermal and mechanical properties of the polymer. The possible structures are head to head (HH), head to tail (HT) and tail to tail (TT). The HH and TT structures coexist together and it is not possible to have a PPC only with one of these two structures. On the other hand, HT configuration is the only type that can exist without any other configuration [17]. The effect of these configurations on polymer characteristics such as glass transition temperature and tensile strength has been studied elsewhere [42-45]. The mechanism of decomposition for PPC in influenced by its molecular weight, ether linkages in the backbone, the decomposition environment and backbone structure. Inert environment promotes chain unzipping whereas in oxygenated environment, chain scission is the main mechanism of decomposition [46]. A combustion reaction due to the presence of oxygen in oxygenated atmosphere makes decomposition faster in air [46]. Regiostructure of the backbones could affect decomposition too. The most common form for decomposition of HT structured backbones is chain unzipping into cyclic propylene carbonate which mostly occurs via either carbonate or alcoxide backbiting. HH and TT regiostructures prevent unzipping mechanism but can go through side-group rearrangement to allow unzipping to proceed. This process takes place at a slightly lower rate [17, 47, 48].

Different techniques were used to improve thermal stability of PPC. Some researchers suggested blending PPC with organic or inorganic fillers or other polymers [49-51]. In other studies, polymerization of the backbone with other component or end-capping of carbonate groups were suggested [52, 53]. Since the focus of this study is to accelerate degradation of polypropylene carbonate, none of these methods are going to be discussed here.

On the other hand, several studies have been performed in order to accelerate degradation of PPC and lower its degradation temperature [17, 54]. By adding photosensitive additive to PPC and exposing the mixture to UV light, thermal stability of the polymer will be reduced [54]. Photo-acid generators (PAG), such as diphenyliodonium or triphenylsulphonium salts, make PPC UV-sensitive and could lower its decomposition temperature. PAG will be decomposed to an organic cation and make a strong Bronsted acid. This acid can attack the backbone of PPC and accelerate its degradation [54]. Polycarbonates are acid sensitive and their degradation in the presence of acid

could occur faster [55]. Other components known as thermal acid generators (TAG), which are activated by heat, could be added to PPC for its catalytic effect on degradation. The mechanism would be the same as PAG [55]. It should be considered that for very low concentrations of acid generators, gas bubbles will nucleate and grow in the polymer when the film is UV exposed. These bubbles make polymer foams and will expand the volume of polymer. In making electrodes, bubble forming should be inhibited[17].

2.4 Porosity measurement

The void space present in the solids is described as porosity, which is a morphological characteristic that is independent of the material [56]. Several methods, based on pore size, could be used for porosity measurement. The following graph (figure 2-4) shows different type of porosity measurement methods.

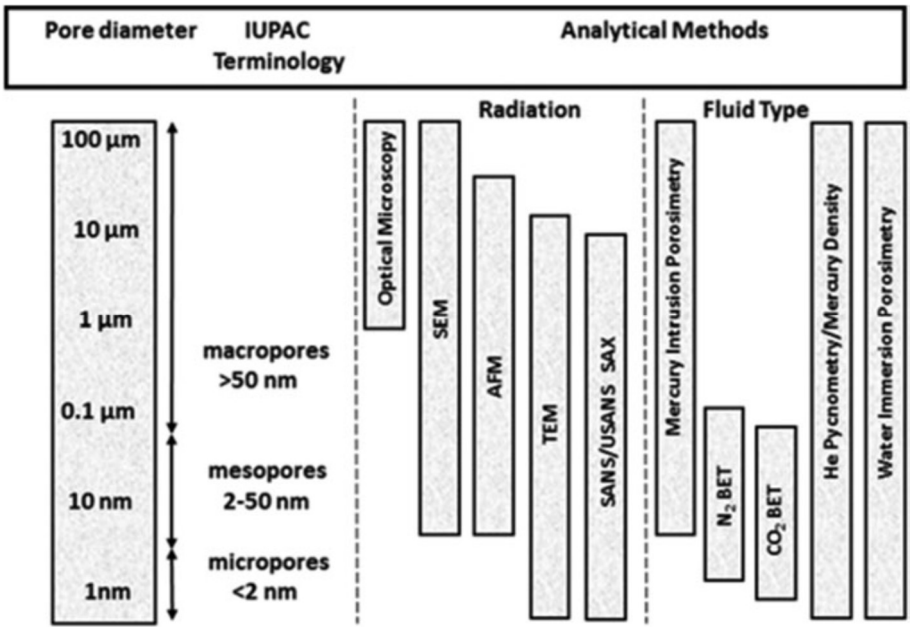

Figure 2-4. Methods for pore size and pore size distribution measurement [57]

Imaging methods such as optical light microscopy, scanning electron microscopy (SEM) with energy dispersive X-ray spectroscopy (EDX), field emission scanning electron microscopy (FESEM) and transmission electron microscopy (TEM) are some of the useful techniques for understanding porosity nature. The abovementioned techniques are 2-dimensional imaging systems. 3-dimensional analysis techniques including atomic force microscopy (AFM) and nuclear

magnetic resonance (NMR) are also available for porosity measurement. Imaging methods coupled with computer image processing softwares, such as ImageJ or MIPAR, will provide a wide range of information. Pore size distribution, pore shape and size are among the characteristics that can be obtained by 2D imaging methods [57]. Among these techniques, SEM will be discussed and used in this study.

2.4.1 Scanning Electron Microscopy

Dimension, shape and size of the pores in porous materials can be obtained by image analysis coupled with SEM. Image analysis softwares use mathematical morphology algorithm to create a pore size distribution for a sample. The most important parts in image analysis are correct preparation of the sample and its scanning process, enhancing the image and pixel analysis [57, 58]. The major step in image analysis operation is to achieve a porosity threshold image for the precise measurement of porosity [57]. In MIPAR software, five different methods for choosing threshold exist: basic threshold, range threshold, adaptive threshold, E-M threshold and local threshold. In basic threshold, pixels are selected based on a comparison between their value and a certain pixel value. In range threshold, pixels are chosen if they are in a specific range of pixel values. In this method a minimum and a maximum should be specified. Adaptive threshold chooses pixels based on their relative intensity to the other pixels in their surroundings. Pixels in E-M threshold are chosen whether they are in a region in which neither of its pixels have fallen below a threshold pixel value distance from the nearest local maximum. Local threshold needs a B/W Companion image and select pixels based on the defined criteria for that image [59].

Porosity measurement by SEM in affected by different factors. Porosity threshold, pore shape and a small region selection could affect the calculations. The preparation of specimen could be effective in the results. If the samples are not conductive, they should be coated with an electrically conductive material with a very thin thickness. If not, during scan, sample with be charged and change the direction of electron beam. The main benefit of using SEM in comparison to optical microscopy is the high magnification that it would reach. But it is usually accompanied with an underestimation of the pore size since it can only detect the pores on the surface and not the whole pore volume [57].

2.4.2 Mercury Intrusion Porosimetry (MIP)

MIP is a porosimetry method which can detect pores in the size range of 3.5 nm to 500 μm. With this technique, pore size distribution, total porosity and the bulk and apparent density could be measured. It should be noted that this technique only provides the largest entrance of the pores and the inner pore size cannot be measured. The following figure 2-5 shows different type of pores. Since there could be no entrance to the closed pores, they also cannot be measured by MIP [60].

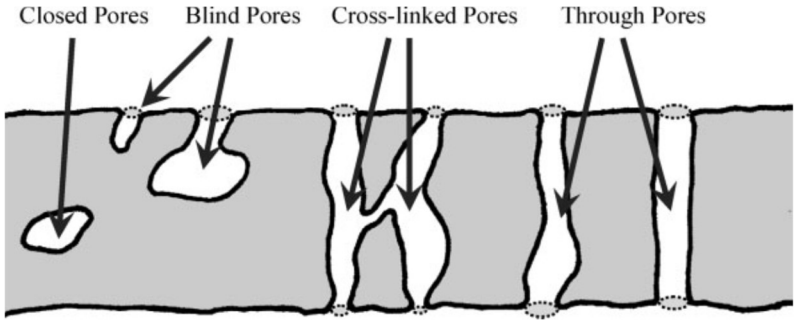

Figure 2-5. Various pore types[60]

The main hypothesis that is used in MIP is that the pore shape has cylindrical geometry. The pore size is governed by Washburn equation which is as follows:

$$\Delta P = \gamma\left(\frac{1}{r_1}+\frac{1}{r_2}\right) = \frac{2\gamma\cos\theta}{r_{pore}}$$

In which, ΔP is the pressure difference between in the curved mercury interface by characteristics of r_1 and r_2. r_1 and r_2 are geometrical parameters that are indicative of curvature of the interface. are the γ and $\cos\theta$ are mercury surface tension and the contact angle between mercury and the sample, respectively. Typical value for γ is 485 mJ/m^2 and for θ is 140° [61]. By having these values, pore size can be measured. However, this equation only gives an estimation of the pore size and pore shape, in reality it could be entirely different from cylindrical pore shape [60].

Since porous materials could easily absorb water or any other chemicals, evacuation of sample is needed before doing the test. Some errors in pore size measurement could occur due to the intrusion of mercury between sample films or inter-particle area of sample granules.

The main procedure for MIP measurements includes two steps. After cell evacuation in order to remove air pockets from sample, the cell is filled with mercury under reduced pressure. By gradual

increase of pressure, the biggest pores or the inter-particle area will be filled. Starting at around 3000 Pa, pore size data is captured. However, lower pressures could be used for starting measurement but it should be taken into consideration that a cylinder with 1 cm height would sense 1333 Pa from the mercury weight. Therefore a sample in a cylindrical cell with 1 cm height will have a pressure difference of 1333 Pa only because of the mercury weight [60]. Pressure in low pressure filling could reach to several atmospheres. Then, by applying isostatic pressure to the sample, total pressure can go up to 414 MPa [56]. The pressures are related to the intruded volume of the sample and pore size and volume can be calculated. Density of the material could also be calculated with MIP with rough estimation (2 to 5%). Pore size distribution of sample is one of the important data that could be derived from MIP. Typically, larger pores are related to inter-particle voids of material and smaller ones are the porous sections inside sample [60].

Although MIP could result in a vast range of data related to material porosity, it is a highly expensive test and very toxic [56]. That is why other imaging techniques test would be preferable to MIP.

2.4.3 Techniques for total porosity measurement

Other simpler techniques are available to measure total porosity of the sample. Gravimetry is a method that results in total porosity, without giving any specific data about pore size and pore size distribution and is measured by the following equation[62]:

Equation 2-1

$$\Pi = 1 - \frac{\rho_{porous\ material}}{\rho_{non-porou\ \ material}}$$

In this Equation 2-1 porous material is the porous electrode and the non-porous material in the base compound for electrode before degradation. For calculation of the volume, length, width and thickness of the sample film will be measured and by dividing mass weight to volume, density of each sample will be calculated.

Liquid displacement method is another technique for porosity measurement. By choosing a proper solvent, that has a reasonable wetting ability to penetrate to the pores, this test can be done. In fact, sample will be immerged in a cylinder filled with a liquid and the volume change in solvent can

be calculated. The volume of the liquid absorbed can be related to the total porosity in the sample [56].

Another method for porosity measurement by highly wetting solvent is called liquid saturation method. With this technique, the porous material is immersed in the liquid. The difference between the weight of dry and wet sample is indicative of porous part of the material. By converting the mass of the solvent to volume, total porosity of the sample will be calculated which in equal to total volume of the solvent divided by volume of the sample. This method basically follows Archimedes principle [63].

CHAPTER 3 EXPERIMENTAL

The experiments were performed in different stages. First, the decomposition in presence of catalysts in small amounts was studied. Then compounding with active ingredients and decomposition under Infrared lamps were performed.

3.1 Materials

3.1.1 Polymers

Sacrificial agents in this study are two polypropylene carbonates, QPAC 40 in pellet form by Empower materials and Converge polyol 212, which is a liquid oligomer, by Novomer company. Molecular weight of QPAC 40 is between 100000 and 300000 g/mol and that for Polyol 212 is about 1000 g/mol. They were both received from Hutchinson company and used as they were. For matrix, two hydrogenated acrylonitrile butadiene elastomers were chosen, Zetpol 2010 with 35 to 37% of acrylonitrile and Zetpol 0020 with 50% acrylonitrile content by Zeon Chemicals L.P., which were used as received.

3.1.2 Catalysts

3 different catalysts were used to study their effect on decomposition temperature. Luperox® 101XL45 (2,5-Bis(*tert*-butylperoxy)-2,5-dimethylhexane) (peroxide), 2,4,5-trichloronbenzenesulfonic acid potassium salt (thermal acid generator or TAG) and Diphenyliodonium hexafluorophosphate (photo acid generator or PAG) by Sigma-Aldrich.

3.1.3 Solvents

To study the effect of catalysts on polymers separately, the various ingredients were mixed at different weight percentages in solvents. Anisole or methoxybenzene by Sigma was the primary choice for solvent which is mentioned in references [54]. For better solubility, THF, also by Sigma, was used.

3.1.4 Active ingredients

Active ingredients in a lithium ion battery electrode can make insertion/disinsertion of lithium reversible within the electrode. Very high percentages of these materials are added to have higher

capacities [7]. They are all in the form of powder. All active ingredients were received from Hutchinson Company and used as received. Graphite is the main ingredient for anodes and the type which was used in this study was graphite AGP-6 by BTR new energy materials INC. The other active ingredients for anode are Lithium titanium oxide (LTO) and carbonated lithium titanium oxide (CLTO) which were obtained by John Matthey. The last active material, which is used in cathode is lithium iron phosphate (II) (LFP) which was provided by Sigma.

To make electrodes conductive and to have good mechanical properties, Carbon black was added [7]. The grade used in this study was SUPER C65 by TIMCAL.

3.2 Methods

3.2.1 Polymer/catalyst solutions

To observe the effect of catalysts on polycarbonate degradation, they were dissolved in a solvent with polymers. Catalysts were added between 1 to 3 weight% to polymers in a 20 wt% solution of polymer/catalyst in solvents. For better solubility, the mixture was put in a sonicator for 1 hour. After dissolution, a film was made and left in air for 24 hours to dry the solvent.

3.2.2 Compounding and electrode film production

To study the effect of catalysts on polycarbonate/HNBR compounds at the same time, a masterbatch with a composition of 6wt% HNBR, 33wt% QPAC 40 (PPC solid) and 61wt% Novomer 212 (PPC Liquid) was prepared in a 200 ml Brabender mixer. First, PPC solid and HNBR were mixed at 60°C and 50 rpm. Since PPC liquid is a very viscous liquid and adding all of it at the same time might not give a homogenous result, it was added gradually to the mixture. By increasing the amount of PPC liquid, glass transition of the compound decreased. To avoid adhesive behavior, the operation temperature decreased. It went as low as 30°C.

In a smaller Brabender mixer, active ingredients were added separately to the HNBR/PPC mixture at 70°C and 30 rpm rotation speed and were mixed for 10 min. Their content was 10 and 20 vol% of the primary compound.

Films with thicknesses between 50-200 μm were made using Calendering technique. Obtained films were put under infrared heating lamps either applied on a Teflon paper or on metal sheets

(Copper or Aluminum). If applied on a metal sheet, films can work as electrodes and were pressed at 100℃ for 5 min before decomposition.

3.2.3 Thermogravimetric Analysis (TGA)

TGA is a thermal analysis method based on measuring the mass variation in a sample while temperature changes. Sample is under a defined atmosphere (nitrogen or air). The mass variations could be due to decomposition, oxidation, or loss of volatiles [64]. In this research, for measuring decomposition temperature and activation energy of decomposition of pure polymers, polymer/catalyst mixtures and compounds, thermal gravimetric analysis was performed using TGA Q500 (TA Instruments, USA). The heating rate in all TGA experiments was of 10℃/min and samples were heated under air up to 800℃.

3.2.4 Fourier transform infrared (FTIR) and UV-VIS-NIR

To understand the range of infrared light in which polycarbonates absorb light the most, an infrared spectrometer using the method of the Fourier transform was used. The tests were completed using a Spotlight 200 FTIR instrument, equipped with a Germanium crystal ATR, from Perkin Elmer (Waltham, MA), with a resolution of 4 cm-1 and an accumulation of 16 scans. The wavelength range which is covered in this test is between 2500-28000 nm.

Since FTIR only covers wavelengths above 2500 nm, UltraViolet-visible-Near Infrared spectrophotometry was performed to have a full spectrum of light absorption for polycarbonates. For this purpose, Cary 7000 Universal Measurement Spectrophotometer (UMS) was used. This equipment gives results in terms of transmittance and reflectance percentages of the samples. By subtracting these two amounts from 100, the absorption of the samples will be calculated. Samples in this equipment should be in the form of transparent films or sheets. For QPAC 40, a free film by dissolving the polymer in THF and letting it dry for 24 hr in air was obtained. PPCL is a highly viscous liquid. To make a film out of it, it was first put in the oven to reach its melting point. Then it was applied on a Spectralon glass which is a reference material with a reference spectrum. By multiplying experimental reflection spectrum with the Spectralon's, the sample spectrum will be obtained. By putting the sample glass on a fridge and cooling it below glass transition temperature, it can be easily put in the machine.

3.2.5 Compound decomposition via Infrared radiation heating

Infrared emitters were supplied by Heraeus Co. Three different types of lamps with three ranges of effective wavelength were used to provide heat to decompose sacrificial phase. Short wave, fast response medium wave and Carbon (long wave) were the lamps which decompositions were carried out under. Heraeus Carbon infrared emitters are designed with medium wave radiation and offer accelerated reaction times. Short wave emitters offer similar range of spectrum to halogen emitters but with better lifetime, strength and durability. Fast response medium wave emitters cover a spectrum between short wave and carbon lamps. Table 1 give technical data on the above-mentioned lamps. This table was adapted from Heraeus company website[65].

Table 3-1. Technical data of Infrared lamps used for decomposition

Technical data			
Twin tube emitter	**Short wave**	**Fast response medium wave**	**Carbon**
Max. specific power W/cm	< 200	80	80
Max. heated length mm	6400/2400*	6400/2400*	3000
Cross-section mm	34 x 14 23 x 11	34 x 14 23 x 11	34 x 14
Filament temperature °C	1800–2400	1400–1800	1200
Peak wavelength µm	1.0–1.4	> 1.4	2
Max. surface power density kW/m²	200	150	150
Response time s	1	1–2	1–2
* Depending on cross-section			

There is a black surface installed at the bottom of the chamber. The control temperature of the device is taken from the surface to regulate the power of the lamps. Since samples surface could have different energy absorption than the black surface underneath it, a thermal camera (FLIR brand) was used to detect samples temperature directly.

3.2.6 Porosity measurement

3.2.6.1 Scanning electron microscopy (SEM)

By using image analysis based on scanning electron microscopy and digital image processing, porosity of porous electrodes can be measured [66]. Various image processing techniques was used to determine pore size and pore size distribution [58, 67]. In this study, surface and cross section images of polymer electrodes with thickness of 100 μm were analyzed by SEM (FESEM, Hitachi S-4700). For image processing, MIPAR software was used to give pore size and pore size distribution of SEM micrographs.

3.2.6.2 Mercury Intrusion Porosimetry (MIP)

Mercury intrusion porosimetry is a technique which is universally used for measuring pore size and pore size distribution. Samples' porosity is characterized by applying different levels of pressure to the samples soaked within mercury. The applied pressure is needed for intrusion of mercury in the pores and is inversely proportional to the radius of pores intruded by mercury [68]. This technique can measure pore sizes as small as 3.6 nm and as large as 200 μm [69].

Although this technique can not define the pore shapes, it can give the volume density of porous parts of samples [60]. Porous structure of polymer electrodes was determined using an AutoPore IV 9500 instrument (Micromeritics Instrument Corporation, U.S.A.) with a 15-ml penetrometer. Samples were placed into the cup of the penetrometer, which was closed by tightening the cap. The penetrometer and sample was transferred into the pressure chamber and pressure was applied in the range 0.015-220 MPa for measurements.

CHAPTER 4 RESULTS AND DISCUSSION

4.1 Thermal characterization of Polymer

4.1.1 TGA of pure polycarbonates in different environments

Figure 4-1 shows TGA curves of the neat PPCL and neat QPAC 40 under air and nitrogen. As it can be seen from this figure, onset temperature which is the temperature at which degradation starts, under oxidative atmosphere (air) was shifted to lower temperatures for both polymers. In addition, the mechanism of decomposition depends on decomposition atmosphere, polymer molecular weight, ether linkages available in the backbone, and backbone regiostructure [17]. In oxygenated atmospheres, chain scission into combustion products, is the primary pattern for decomposition. In a nitrogen environment, chain unzipping from the ends of the polymer chain or unzipping following chain scission is the main form of decomposition. Ether linkages prevent chain unzipping and higher molecular weight decomposition fragments will be resulted. Regiostructure of the backbones could affect decomposition too. Different mechanisms exist depending on how end groups of each repeating units attached to each other (head to tail (HT), head to head (HH) and tail to tail (TT)). The most common form for decomposition of HT structured backbones is chain unzipping into cyclic propylene carbonate which mostly occurs via either carbonate or alcoxide backbiting. HH and TT regiostructures prevent unzipping mechanism but can go through side-group rearrangement to allow unzipping to proceed. This process takes place at a slightly lower rate [17, 47, 48].

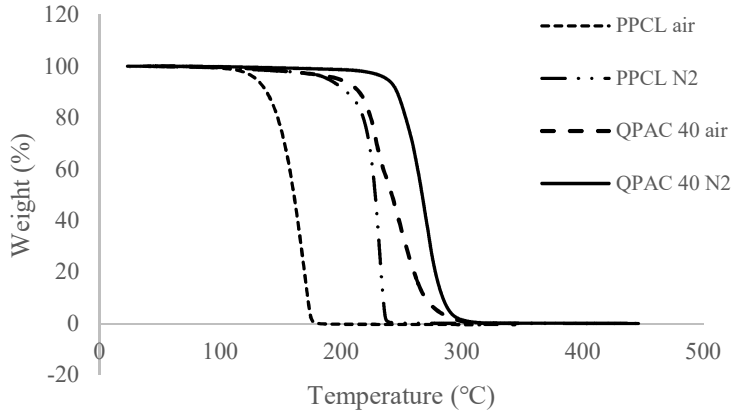

Figure 4-1. TGA graphs of neat PPCL and QPAC 40

The difference between degradation under nitrogen atmosphere and oxygen was studied elsewhere [70]. There are some differences in the initial steps. Oxygen will ease branching and radical formation by forming peroxide active sites. Peroxides will produce aldehydes, ketones and branched structures, mostly in the first stages of degradation [70-72]. Formation of peroxide at this stage helps increasing the rate of degradation under air in comparison to the nitrogen environment.

Decomposition of QPAC 40 with higher molecular weight occurs at lower rate and at higher temperature. Lower temperature and higher molecular weight restricts the amount of end groups in the backbone and therefore unzipping does not start until high temperatures [70]. In PPCl, main degradation mechanism is chain unzipping after a small step of chain scission. For QPAC 40 two stages of high decomposition rate appears in DTGA graph. The first one shows the region in which chain scission mechanism is dominant and the second one, at higher temperature, is chain unzipping dominant region (Figure 4-2).

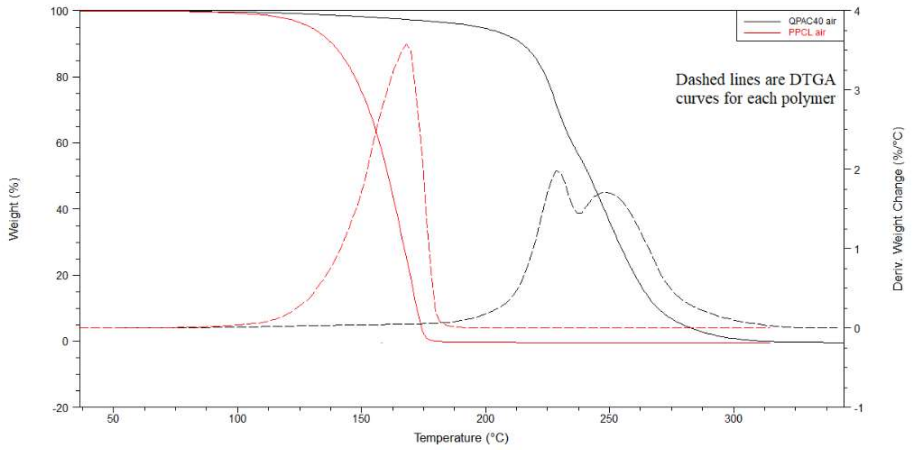

Figure 4-2. DTGA curves of PPCL and QPAC 40 under air

4.1.2 Thermal degradation of HNBR

To set a limit for the highest temperature in the decomposition process, a TGA test was performed on pure HNBR under air. Onset temperature of pure HNBR in oxygenated environment was calculated from TGA curve and is equal to 397 ℃. In the presence of 1% peroxide catalyst, onset

temperature of HNBR increased to 405 ℃, which shows that the catalyst did not have a negative effect on the matrix.

4.1.3 Catalyst effect on thermal degradation of polycarbonates

Peroxide formation in the first stages of degradation under air was shown elsewhere to be effective in increasing the degradation rate of polycarbonates [70]. To see if adding excess peroxide could positively affect QPAC and PPCL degradation, Luperox was added to them between 1 and 3 wt% and put in TGA equipment under air environment. Also, PAG and TAG were added to the polycarbonates to study their effect of degradation. Figures 4-3 and 4-4 show the results of TGA for PPCL and QPAC respectively under air in the presence of each catalyst.

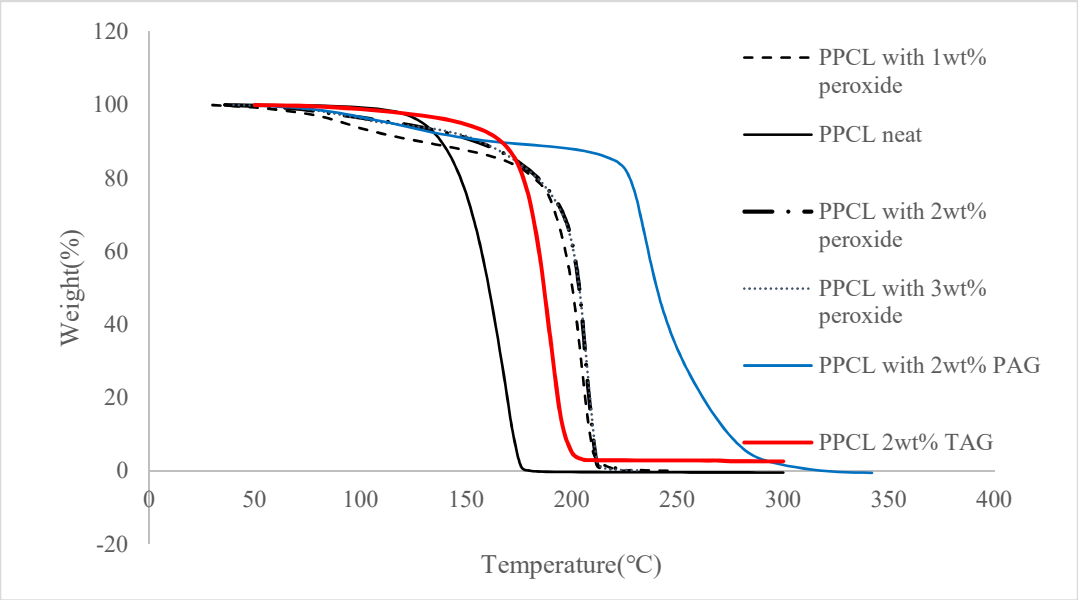

Figure 4-3. TGA curves of PPCL under air with different catalysts

As it can be seen from Figure 4-3 and Figure 4-4, none of the catalysts decreases the onset temperature of PPCL and QPAC. In PPCL, all three catalysts increased the degradation temperature. As it can be seen from Figure 4-3 in case of peroxide and TAG, decomposition started at higher temperatures, but the weight loss rate is the same as the neat polymer. For the PPCL compound with PAG, weight loss rate is different from the neat polymer. It can be said that excess peroxide and generated acid available in the system reacted with the peroxides that formed during degradation and prevented degradation until higher temperatures. Therefore, chain scission in first

step, which is the primary form of degradation, is inhibited and the mechanism of degradation is mostly chain unzipping. In QPAC also, peroxide, TAG and PAG increased degradation temperature. The polyethers available in this polymer react with the generated acid from PAG and TAG and excess peroxide and by generating an alcohol ending in the chain, unzipping of QPAC chain is delayed [17].

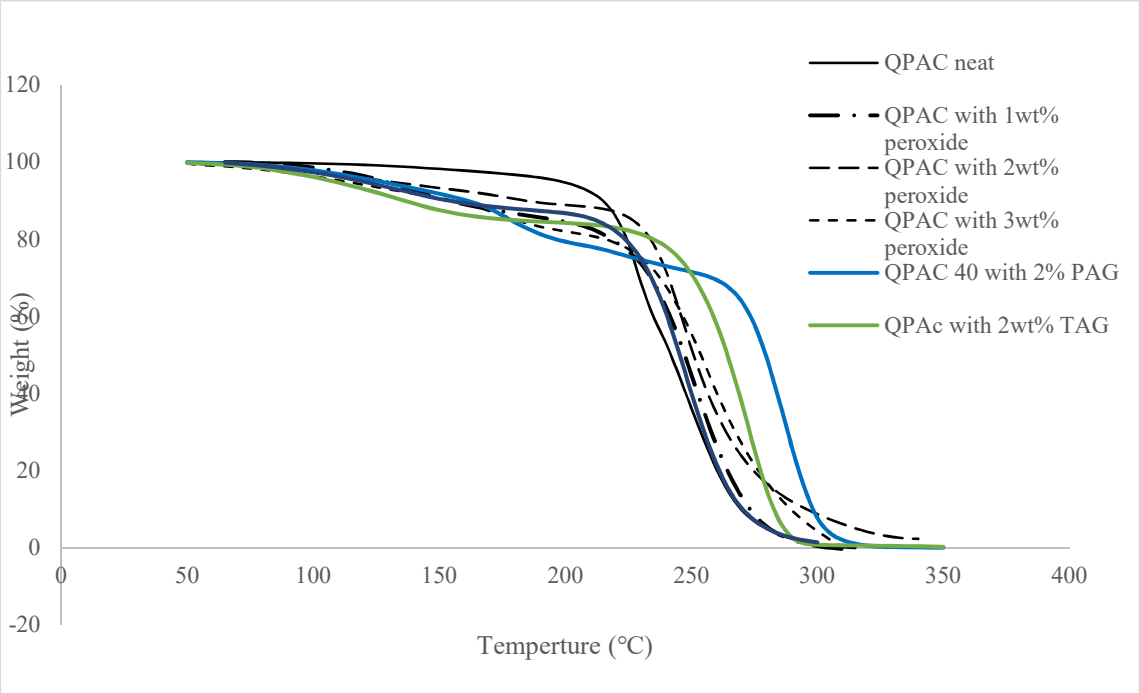

Figure 4-4. TGA curves of QPAC under air with different catalysts

4.1.4 Energy of decomposition via Coats-Redfern method

To calculate the energy of decomposition in polymers, the following method was used: The reaction rate can be expressed by multiplying a function which is temperature dependent, (here K(T)) and a composition- or conversion- dependent term,

$$d\alpha/dt = K(T)f(\alpha)$$ Equation (4-1)

In this equation α is the conversion (weight of polymer consumed in the reaction/initial weight of polymer), t and T are time and temperature respectively. K(T) is the rate of reaction, which is considered to have an Arrhenius type relationship.

$$K(T) = Aexp(-E/RT)$$ Equation (4-2)

A, E and R are the pre-exponential factor, the activation energy of reaction and the universal gas constant, respectively. Polymer degradation reaction can be assumed as a simple nth-order reaction and can be a function of conversion as shown in Equation 4-3.

$$f(\alpha) = (1-\alpha)^{n}$$ Equation (4-3)

By combining these 3 equations and assuming that the heating rate β, is constant, a new expression will be obtained

$$\frac{d\alpha}{dT} = \frac{A}{\beta}(1-\alpha)n\ exp(-E/RT)$$ Equation (4-4)

All of the expressions that are offered for calculation of kinetic parameters in thermal degradation of polymers are based on Equation (4-4). By integrating this equation and assuming degradation a first order reaction, Equation (4-5) will be obtained, in which α_{max} is the degree of conversion at the inflection point and T_{max} is the inflection point temperature in DTGA curve. This equation is called Kissinger and Ozawa equation.

$$ln\frac{\beta}{{T_{max}}^2} = ln\left(\frac{A.R}{E_a}\right) - \frac{E_a}{R.T_{max}}$$ Equation (4-5)

By obtaining T_{max} and α_{max} for different heating rate and plotting the left side of equation 4-5 versus $1/T_{max}$, E_a and A will be obtained.

Another expression is available for the calculation of activation energy and pre-exponential factor, which has the benefit of using only one set of data with one heating rate. This equation is called Coats-Redfern Equation and is expressed in Equation (4-6)

$$ln\left(\frac{-ln(1-\alpha)}{T^2}\right) = ln\left(\frac{A.R}{\beta.E_a}\right)\left(1-\frac{2.R.\bar{T}}{E_a}\right) - \frac{E_a}{R.T}$$ Equation (4-6)

By plotting left side of this equation vs. -1/T, activation energy and pre-exponential factor will be calculated. Table 4-1 shows the onset temperatures and kinetic parameters calculated by Coats-Redfern method for pure and catalyst-containing samples. As it can be seen from this table, for pure polycarbonates, nitrogen inhibits oxygenation of the polymers at lower temperature and degradation temperature and energy are much higher than in air environment.

All catalysts increased activation energy to much higher amounts in comparison to pure polymers. These results confirm that these catalysts not only did not help reducing the degradation temperature, but they also worked as a kind of stabilizer of polycarbonates and slowed down the degradation reaction. For this reason, they were not added to the blends for further investigations.

Table 4-1. Pure and catalyst-containing polycarbonates kinetics parameters calculated using Coats-Redfern method for air and nitrogen environment

	Onset T	Energy of Decomposition (J/mol)	A
PPCL air	148	136000	$2.1*10^{14}$
PPCL N2	221	258000	$6*10^{16}$
QPAC N2	250	195000	$4.58*10^{15}$
QPAC air	218	158000	$1.92*10^{7}$
PPCL 1% peroxide	193	310000	$2.27*10^{23}$
PPCL 2% peroxide	198	213667	$2*10^{21}$
PPCL 3% peroxide	196	236000	$9*10^{23}$
PPCL 2% TAG	178	242000	$1.96*10^{25}$
PPCL 2% PAG	223	145000	$2.43*10^{12}$
QPAC 40 1% peroxide	220	160000	$5.5*10^{13}$
QPAC 40 2% peroxide	242	187000	$1.01*10^{16}$
QPAC 40 3% peroxide	226	227000	$2.9*10^{20}$
QPAC 40 2% TAG	259	177000	$4.74*10^{14}$
QPAC 40 2% PAG	223	160000	$2.5*10^{12}$

4.1.5 Thermal degradation of primary compounds

After studying thermal degradation of polymers either in pure state or in the presence of catalysts, blends of a polymer with active ingredients were prepared to analyze the effect of each additive on degradation of polycarbonates. First, a blend of PPCL/QPAC/HNBR with a composition that was mentioned in section 3.2.2 was made and then was mixed with 10 and 20 vol% of active ingredients. Figure 4-5 summarizes the effect of each active ingredient on the thermal degradation of PPC in terms of T_{onset}. As it can be seen, CLTO decreased T_{onset} significantly which means that polycarbonates degrade faster in the presence of CLTO. LTO also reduced the degradation temperature of PPC but not as effectively as CLTO. It was shown in other studies that titanates promote the degradation of polycarbonates [73]. This is due the high susceptibility of polycarbonates in the presence of alkaline environment at high temperature. Titanates facilitates chain scission which promotes degradation at lower temperature [74].

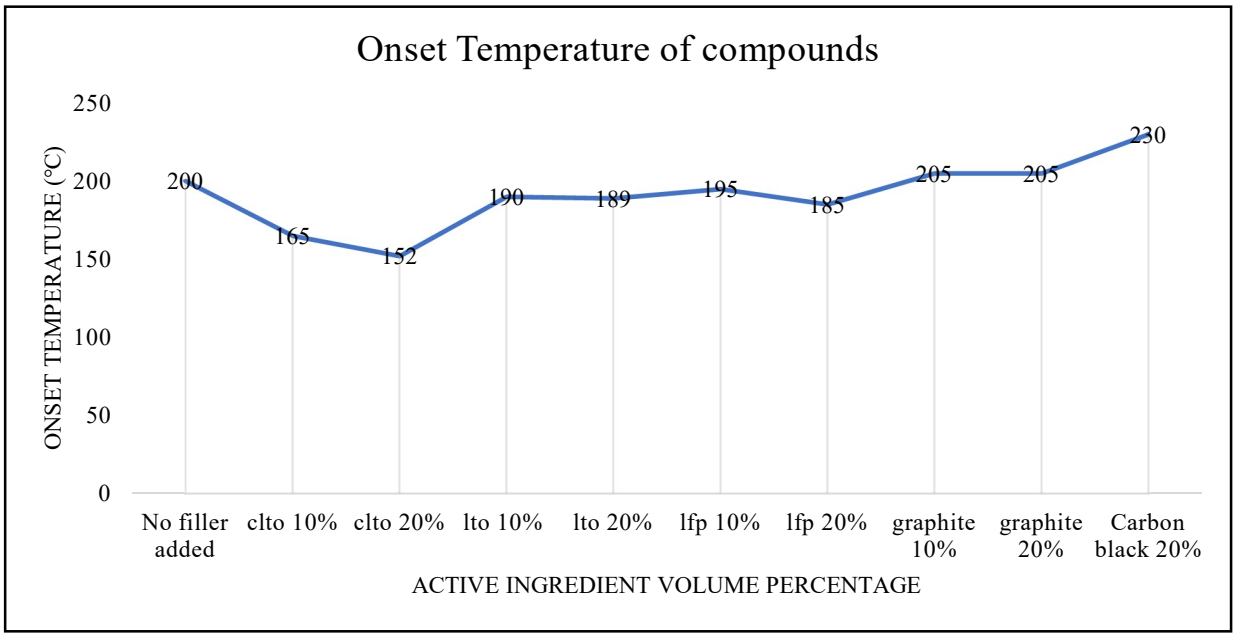

Figure 4-5. Effect of active ingredients on onset temperature of PPC/HNBR compounds

LFP also decreased the decomposition temperature of polycarbonates and by increasing its content, lower degradation temperature is achieved. By using the same reasoning as LTO, it can be said that LFP is also an alkali compound that facilitates degradation of polycarbonates.

The only active ingredient which slowed down the degradation of polycarbonate and increased the onset temperature in TGA experiments is graphite. Graphite layers act as a thermal insulator and delay degradation of polycarbonate. By dispersing graphite uniformly in the polycarbonate, the conduction of heat will take place with more difficultly and the layers make a barrier against the mass transport of generated volatile species The graphite layers, which uniformly disperse in the matrix, lead to the difficulty in heat conduction and act as a mass transport barrier to the volatile products which are generated during decomposition [75].

Carbon black should be added to the electrodes to increase electrical conductivity. Therefore, it can affect the degradation process of polycarbonate and its effect should be studied. As it can be seen from Figure 4-5. Effect of active ingredients on onset temperature of PPC/HNBR compounds by adding 20 vol% of CB to the blend, degradation temperature increased 30°C.

4.2 FTIR and UV-VIS-NIR experiments for polymers and fillers

As it was mentioned in 3.2.4, absorption of light plays an important role in degradation of polycarbonates while using infrared heating. Figure 4-6 shows the FTIR curves of PPCL and QPAC. As it can be seen from this figure, both polycarbonates have almost the same absorption peaks, which is a typical spectrum for polypropylene carbonates[47].

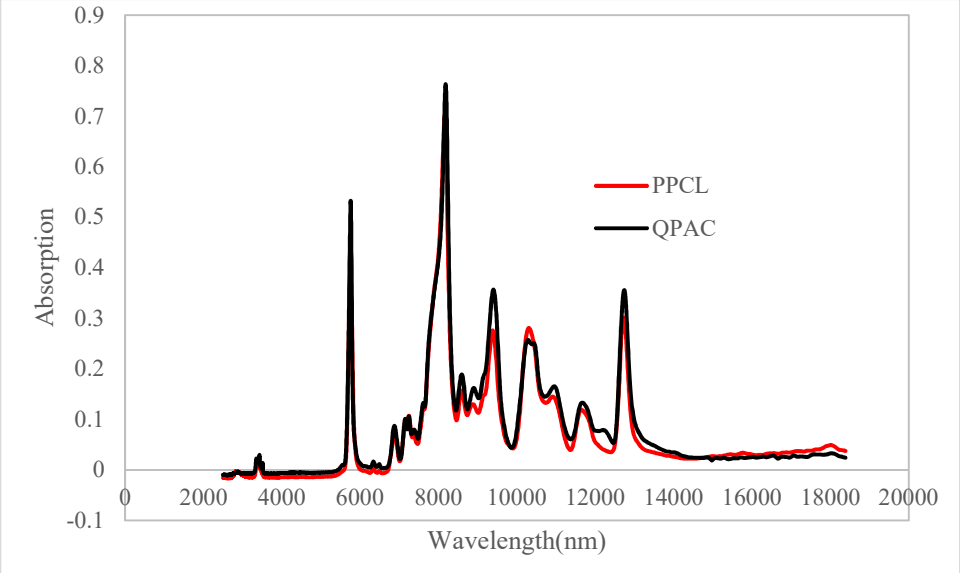

Figure 4-6 .FTIR curves of PPCL and QPAC

Figure 4-7 shows the Spectral radiation curves for different infrared emitters, normalized to the same power (right), and absorption of infrared for some polymers (left). The available infrared lamps in this research are short wave, fast response medium wave and carbon. By comparing FTIR curves and the ranges covered by the lamps, it can be concluded that the wavelengths studied by FTIR is not sufficient for choosing the best theoretical lamp for degradation. Therefore, UV-VIS-NIR tests were carried out and the results are presented in Figure 4-8. The results are comparable with what was done before in the literature [76]. By comparing the power peak of lamps in Figure 4-7 and the highest absorption peak of both polypropylene carbontes in Figure 4-8, it can be concluded that the carbon lamp would be the best option for degradation, which Heraeus Co. suggested for other polymers.

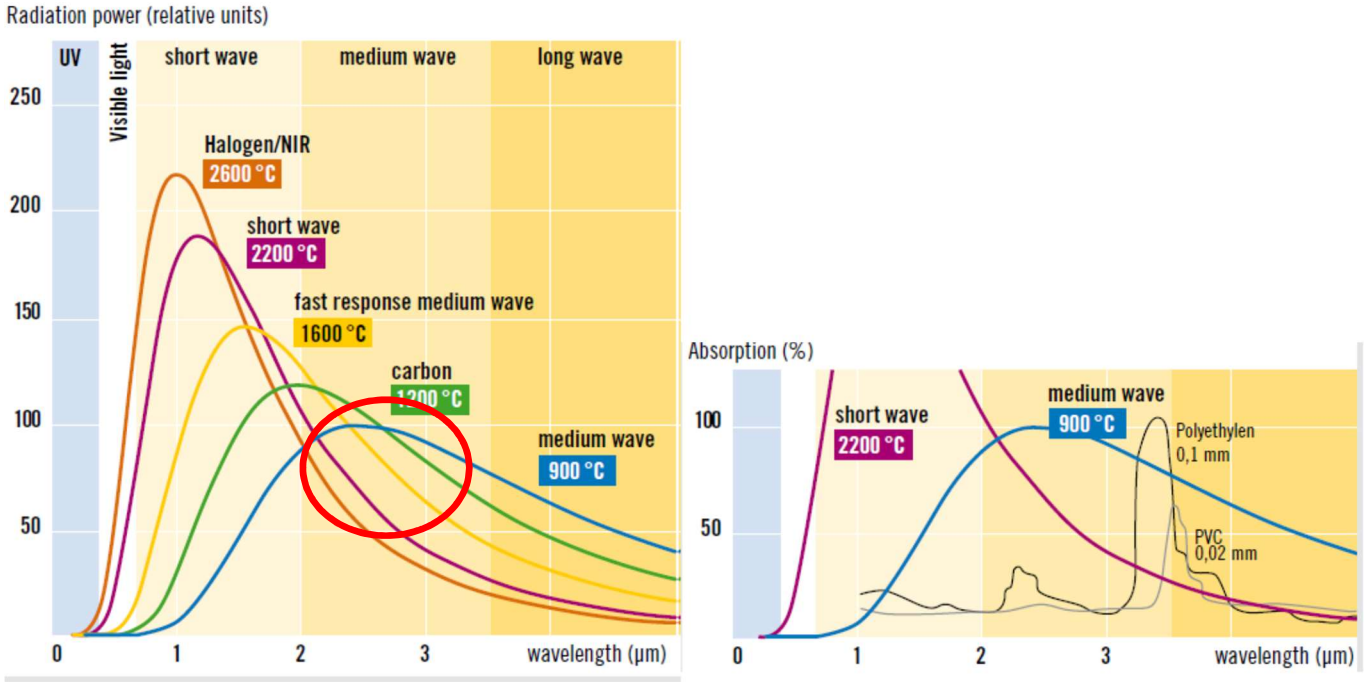

Figure 4-7. Spectral radiation curves for different infrared emitters, normalized to the same power (right), absorption of infrared for some polymers (left)

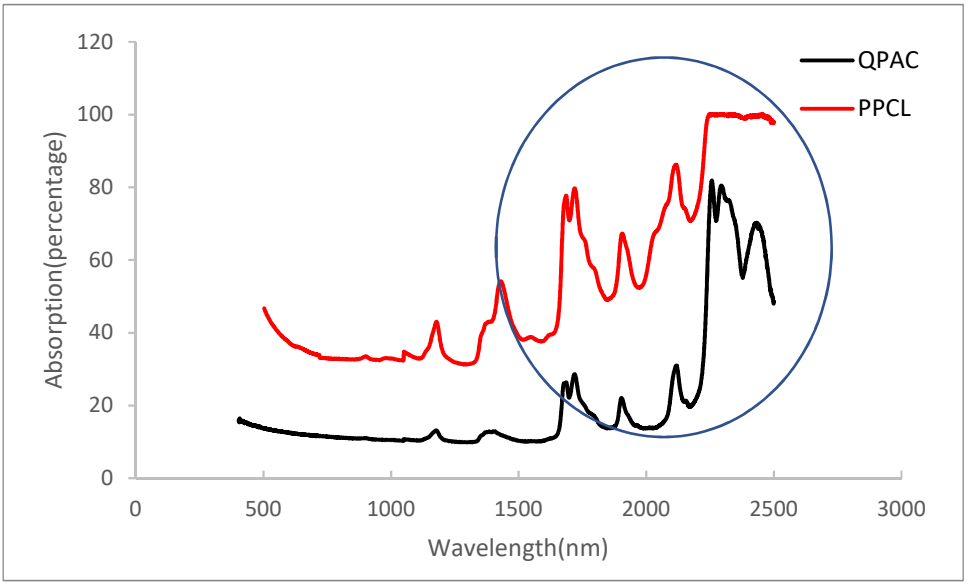

Figure 4-8. Absorption curve of PPCL and QPAC by UV-VIS-NIR

4.3 Degradation of primary compounds by Infrared radiation heating

By having the onset temperatures of primary compounds in section 4.1.5, there is an estimation for degradation temperature and energy required from IR lamps. Compounds were formed into the films with thicknesses between 50-200 µm. Degradation was carried out in isothermal and ramp heating conditions. First, ramp heating was done to imitate TGA conditions with fast response medium wavelength ramp to see the effect of thickness. In this step, thicker samples degradation was slower than the thinner ones since there is more sacrificial phase in the films and higher temperature which can be translated to more time is needed for degradation.

In the next step, for a 100 µm film of compounds containing 20 vol% of active ingredients, all three lamps with ramp method were used. In this step, the most suitable lamp in accelerating decomposition of PPC is chosen.

Since the samples might not have the same absorption as the black surface beneath it, the temperature of sample surface is also recorded. Figure 4-9 shows how FLIR camera records the sample temperature.

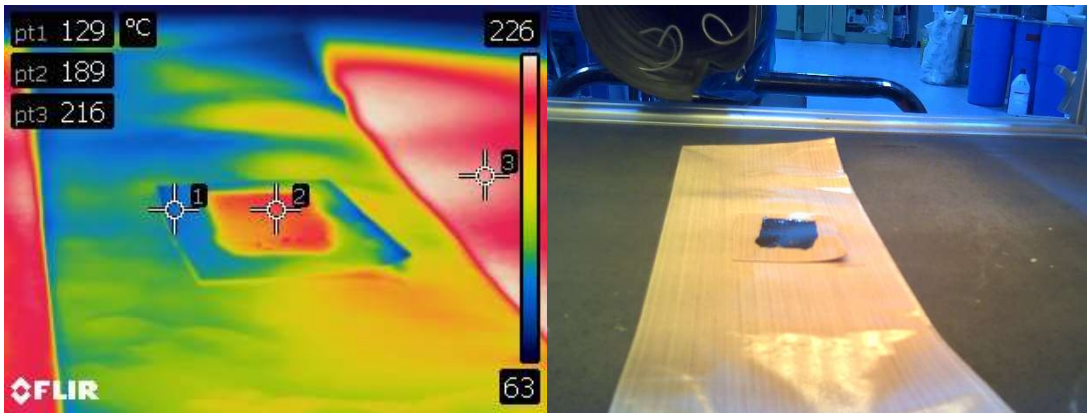

Figure 4-9. FLIR image of the sample while heating under infrared radiation

The results for comparing three lamps are given in Figure 4-10 to Figure 4-13. The difference between sample temperature and thermocouple temperature is also shown in these graphs.

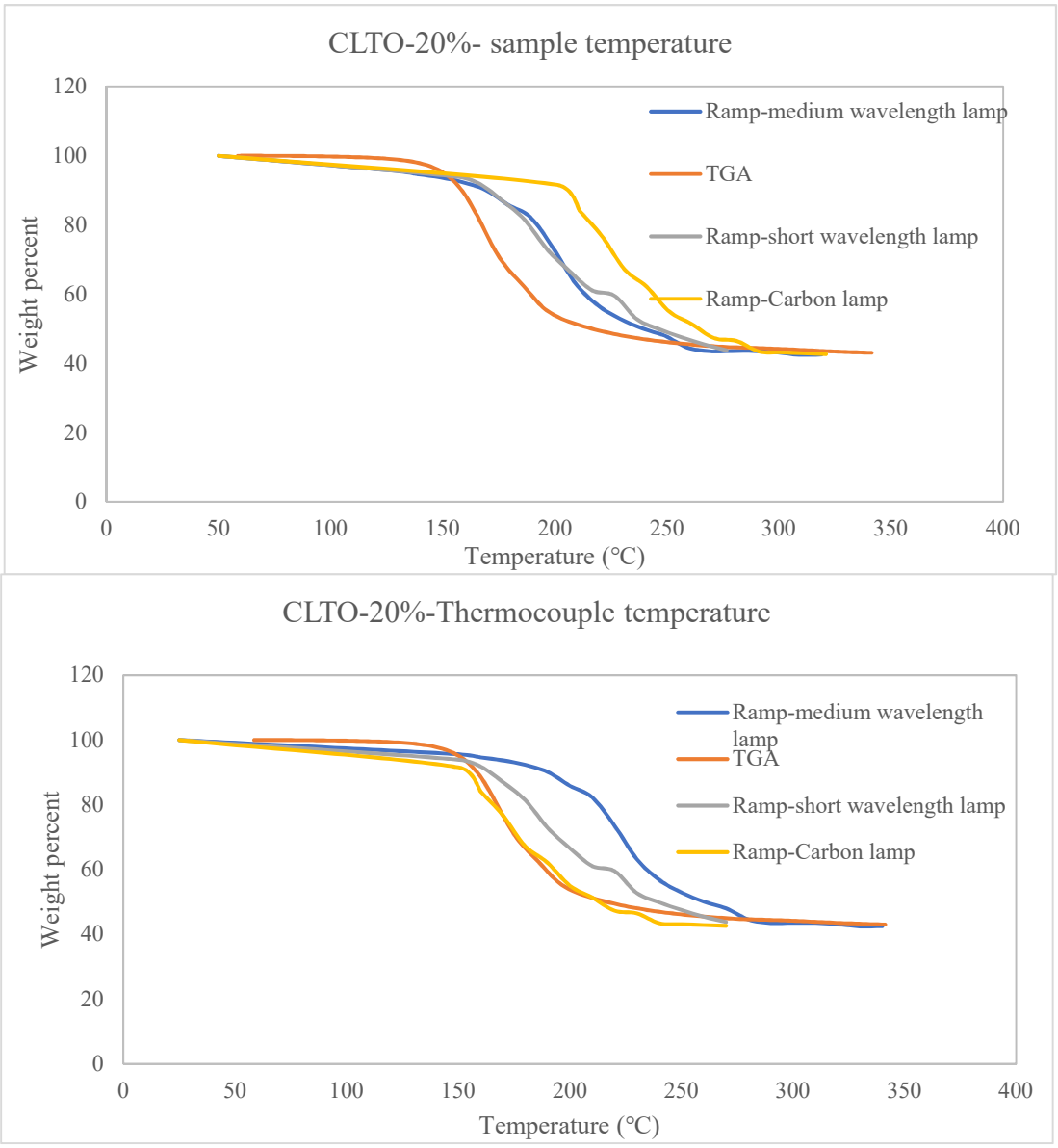

Figure 4-10. Comparison of three lamps for 100 µm film of compounds containing 20 vol% CLTO

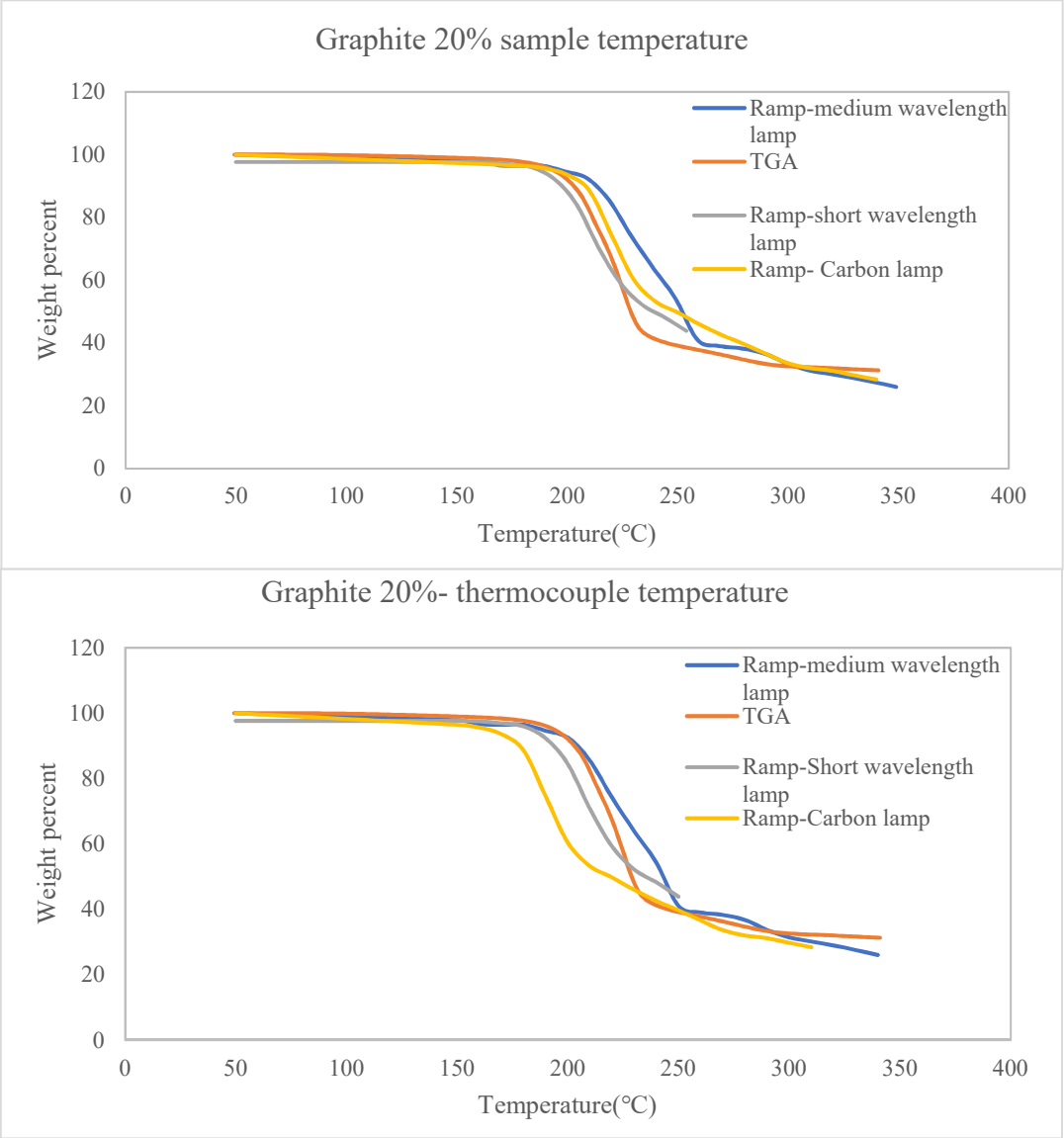

Figure 4-11. Comparison of three lamps for 100 µm film of compounds containing 20 vol% Graphite

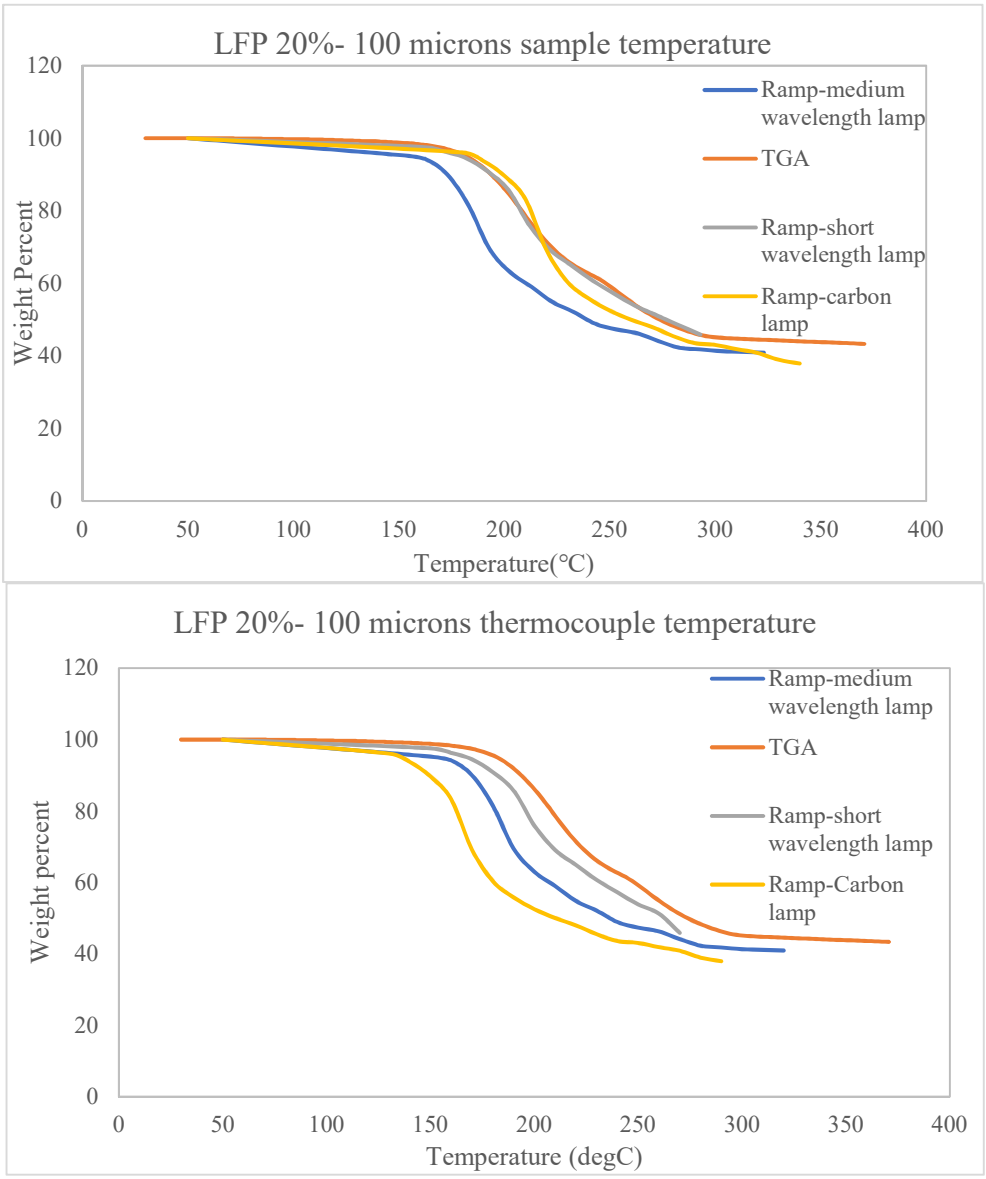

Figure 4-12. Comparison of three lamps for 100 µm film of compounds containing 20 vol% LFP

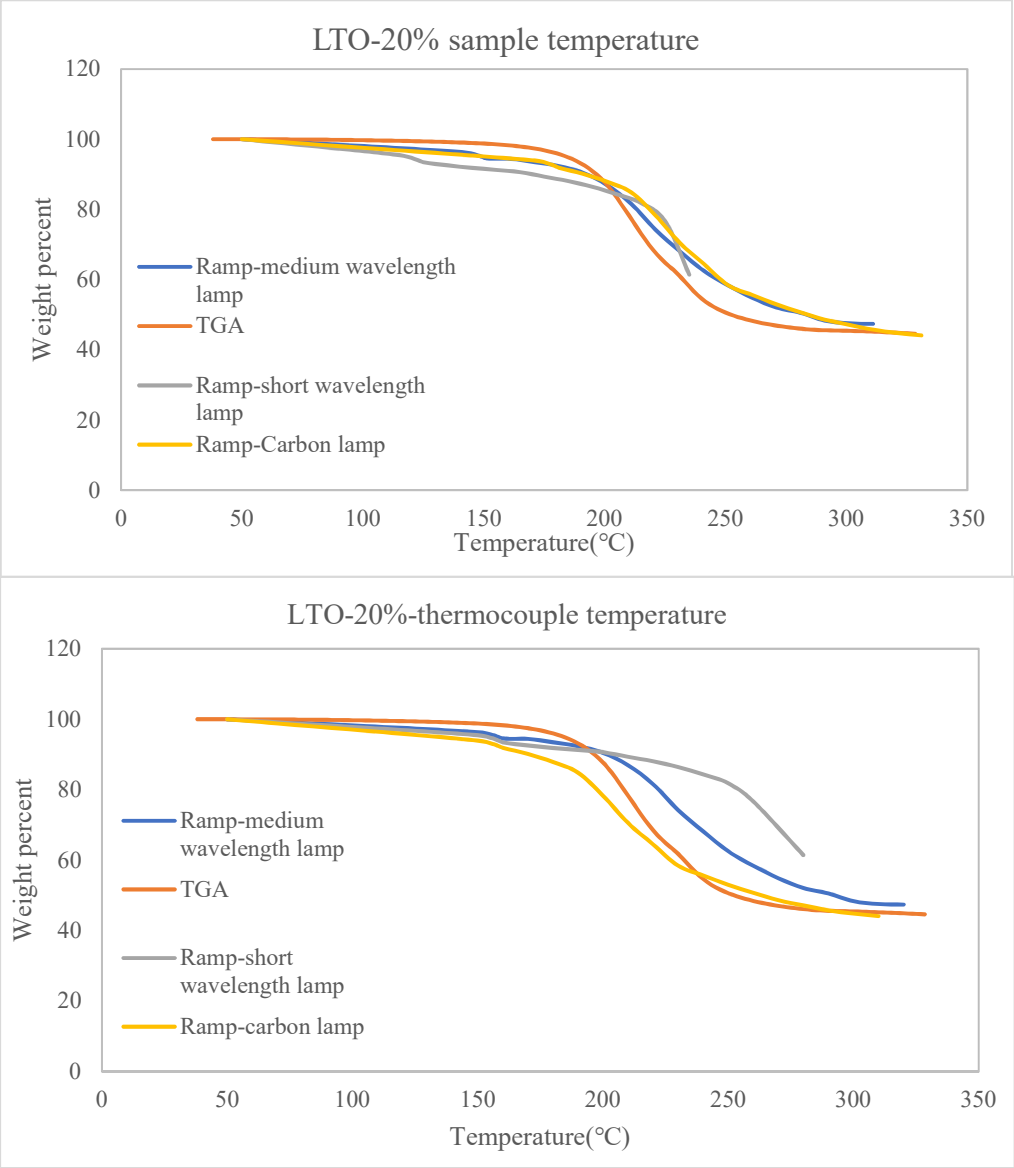

Figure 4-13. Comparison of three lamps for 100 μm film of compounds containing 20 vol% LTO

Short wavelength lamp covers a smaller range of temperature compared to the other two lamps. As shown for example in Figure 4-13, the covered range is not enough for degradation of LTO. Also, since short wavelength lamp energy peak does not have any overlap with PPC, it is the less effective lamp in degradation. By looking at thermocouple temperature in Figure 4-10Figure 4-13, it can be seen that under irradiation of carbon lamp, all compounds start degradation at lower temperature and highest degradation rate is at a lower temperature range in comparison to fast response medium wavelength lamp. On the other hand, by comparison of sample and thermocouple temperature for each compound, temperature increase under carbon lamp is more intense than for the other lamp. It shows the effectiveness of radiation power on samples. Having these results, it can be said that the carbon lamp is the most efficient lamp for degradation. With these graphs, it is possible to figure out the range of temperature in which degradation is at its highest rate.

After obtaining a temperature range from thermocouple graphs in which the highest decomposition rate occurs, isothermal tests were carried out at constant temperatures for different durations to reach full degradation. Isothermal tests were done for films with 50 and 150 µm thickness and stopped after degradation reached a plateau.

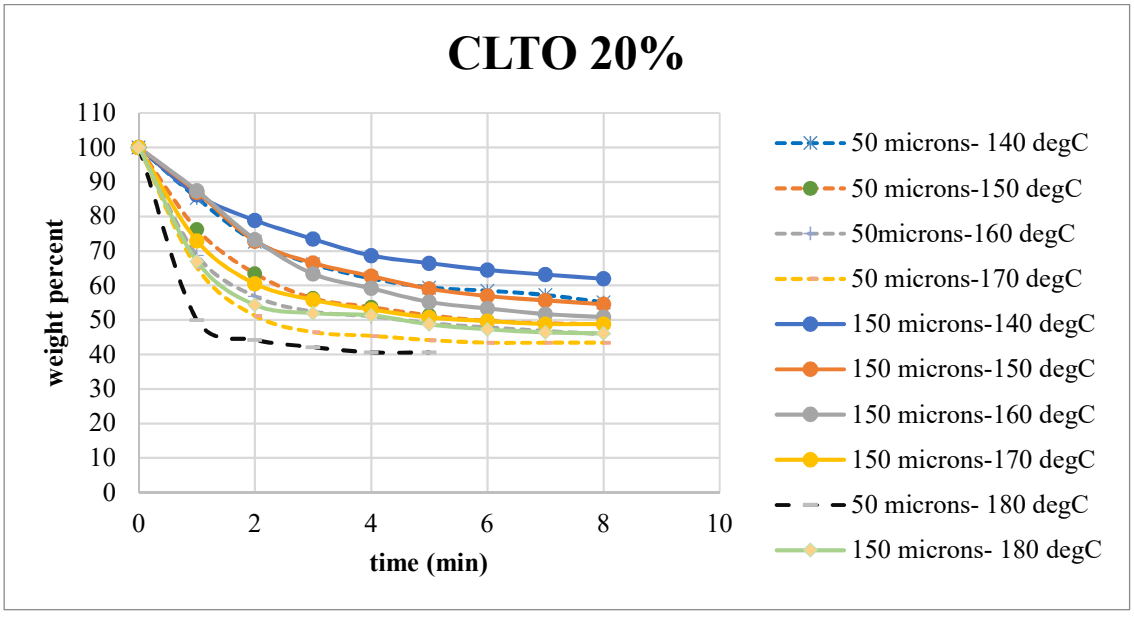

Figure 4-14. Isothermal degradation of compound containing 20vol% of CLTO at two thickness and different temperatures

For a compound containing 20 vol% CLTO, the temperature range in which degradation rate is at its highest is between 140 and 180℃. This compound has PPC content of 57 wt% and after degradation is complete, 43% of the weight should be remained. As it can be seen from Figure 4-14, for a 50µm film, 180℃ is too high and the degradation is so rapid that the Teflon paper underneath it loses some weight. But 170℃ and 180℃ for 5 min is a good condition for degradation of 50 µm and 150 µm films. The highest temperature recorded by FLIR camera on the surface of the samples was 240℃ and no cracks or bubbles were visible.

Compounds containing 20 vol% LFP and 20 vol% LTO have the same PPC content as compounds containing 20 vol% CLTO which is 57 wt%. Highest degradation rate for LTO compound occurs between 180-220℃ and for LFP compound between 140-190℃.

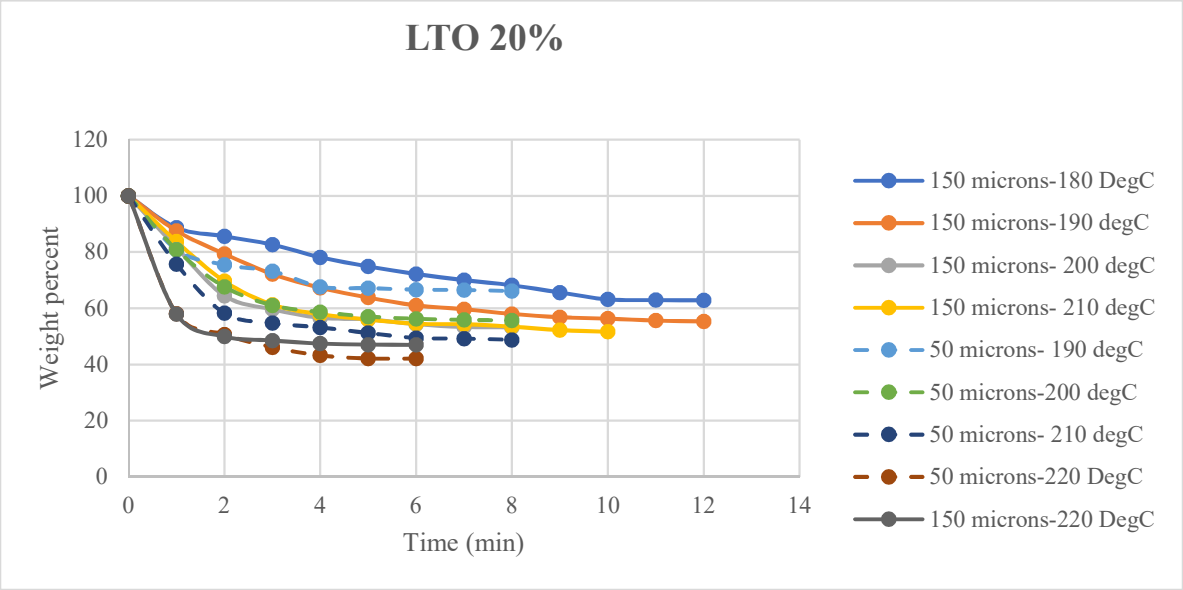

Figure 4-15. Isothermal degradation of compound containing 20vol% of LTO at two thickness and different temperatures

Figure 4-15 shows the isothermal degradation of LTO compound at each temperature in the range mentioned above. LTO has a bright color and less energy is absorbed by it in comparison to other active ingredients. Therefore, higher thermocouple temperature is needed to produce the required energy of degradation. Both 50 and 150 µm films had complete degradation at 220℃ after 6 min and no cracks or bubbles were visible on their surface. Sample temperature goes up to 250℃.

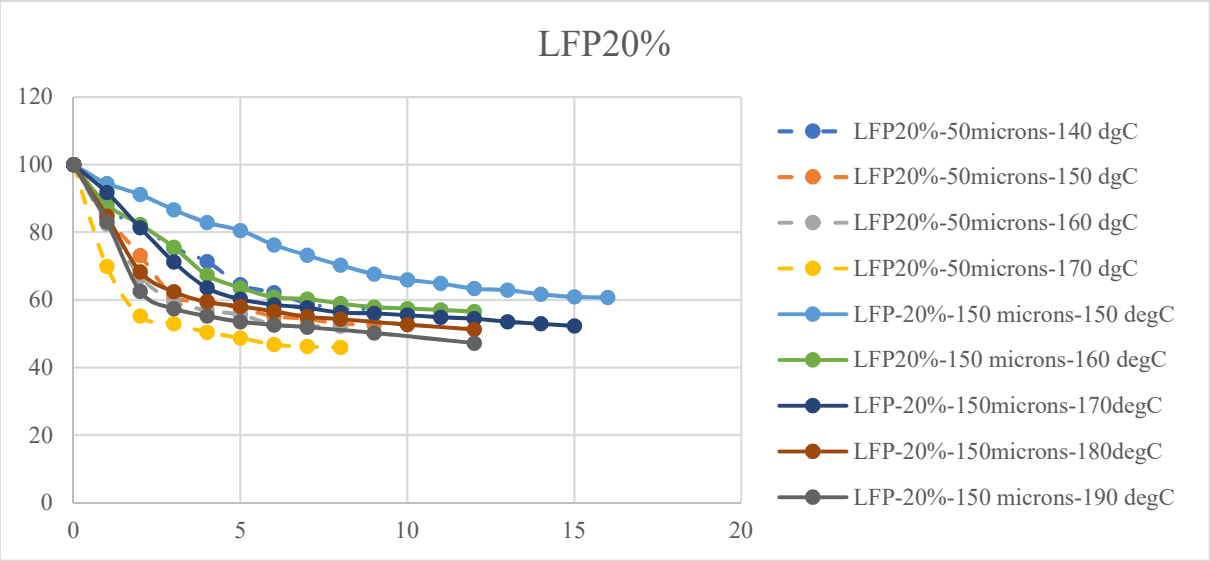

Figure 4-16. Isothermal degradation of compound containing 20vol% of LFP at two thickness and different temperatures

In Figure 4-16, isothermal degradation of LFP compound is shown. For a 50 µm film, after 8 min at 180℃ and for a 150 µm film, 12 min at 190℃ are needed for complete degradation of PPC. The highest temperature recorded by FLIR camera on the surface of sample is 280℃ and no cracks were visible on the surface.

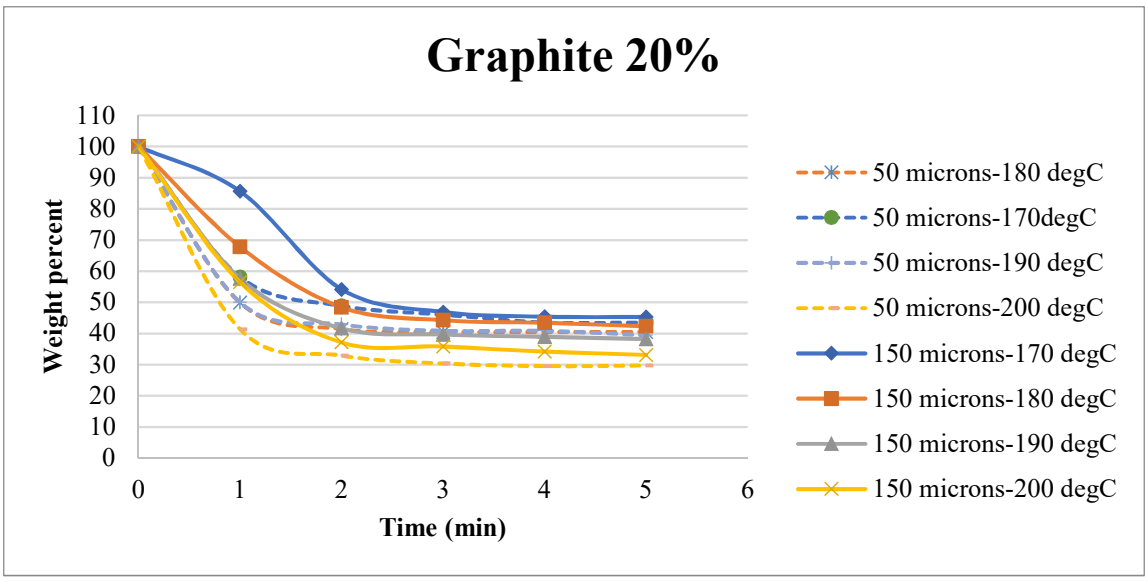

Figure 4-17. Isothermal degradation of compound containing 20vol% of graphite at two thickness and different temperatures

20 vol% Graphite compound has 67 wt% PPC and after degradation 33% of the total weight should be remained. Figure 4-17 shows isothermal degradation of graphite in the range of 170-200℃. Graphite powder has a layer structure and that makes passing of degradation gases through the films harder. Although at 200℃ for 5min of heating degradation is completed, but bubbles and cracks appear on the surface which make the electrode film useless. Bubbles appear due to high degradation rate of PPC and not enough passage available for them to escape the surface. To overcome this problem, lower temperature to achieve lower degradation rate at the beginning of heating can be suggested. Degradation can start at 170℃ and goes up in a ramp to 200℃ and stops when degradation is complete. Graphite is also dissipating energy very intensely at the bottom layers, which makes the Teflon paper beneath it to degrade and deform. The highest temperature recorded for the sample was 280℃.

4.4 Degradation of final electrode compounds

In previous sections, only one active material was added to the compounds to see the effect they have separately on PPC degradation. However, to have an electrode with the highest efficiency for

generating ions and conductivity at the same time, sometimes several active ingredients are added to the compound at the same time. Hutchinson Co. provided seven final electrode compounds to study their degradation under infrared lamps. These compounds also have different matrixes.

G1, G2 and G3 are graphite compounds and have almost the same amount of PPC in them. The only difference in these compounds was their matrix. For G1, G2 and G3 respectively, HNBR Zetpol 0020, EPDM and TPE (Lotader 5500) were used. G4 is also a graphite compound that has the same matrix as G3 but with higher content of graphite. The main active ingredient in LFP1 and LFP2 is LFP but with different matrices and LFP contents. In LFP1, HNBR and in LFP2, Lotader 5500 were used as the matrix. LTO1 is a LTO compound with Lotader 5500 as its matrix. Table 4-3 shows the composition of these compounds.

By combining several active ingredients in one compound, degradation temperatures might change and TGA tests were done on them using a ramp method. T_{onset} of the compounds are shown in Table 4-2.

Table 4-2. Degradation temperature of final compounds

Code	Onset temperature (°C)
G3	250
LFP2	180
G2	240
G1	230
LFP1	170
G4	221
LTO1	160

Table 4-3. Final compounds composition

Code	Active ingredients and their content (wt%)	Binder Type and content (wt%)	Total PPC wt%	Total PPC vol%
G1	Graphite (66)	HNBR (2)	**32**	42
G2	Graphite (64)	EPDM (2)	**34**	45
G4	Graphite (69.3)	**TPE** of ethylene, acrylic ester and maleic anhydride (2.1)	**29**	38
LTO1	LTO (64) and carbon black (5)	TPE (2)	**29**	50
LFP1	LFP (63) and carbon black (5)	HNBR (2)	**30.3**	50
LFP2	LFP (66.7) and carbon black (5.2)	TPE (2.2)	**26**	45
G3	Graphite (64)	TPE (2)	**34**	45

Films with thickness of 100 μm were made from final compounds. Graphite films were applied on copper films and other compounds on aluminum films. They were placed afterwards under hot press for 2min at 90°C for graphite compounds and at 60°C for the other compounds. The films were pressed on the substrate and then were degraded under infrared lamps. The method that was used for all the films, except for graphite ones under IR carbon lamps, was isothermal. For samples containing graphite, a ramp procedure was used to prevent or decrease the amount of bubbling on the surface.

Table 4-4. The summary of decomposition conditions for each final compound.

Code	PPC wt%	PPC vol%	Decomposition Temperature (degC)	Highest sample Temperature	Decomposition time (min)	Maximum reached decomposition
G1	**32**	42	Gradually increased from 150 to 260	290	6':30"	**33%**
G2	**34**	45.3	Gradually increased from 150 to 250	260	6':30"	**34%**
G4	**29**	38	Gradually increased from 150 to 260	255	8':30"	**29%**
LTO1	**27.3**	50	190	255	7':30"	**27.5%**
LFP1	**31**	50	180	250	5'	**31%**
LFP2	**26**	45	180	250	5'	**26%**
G3	**34**	42	Gradually increased from 150 to 250	265	6':30"	**34%**

LTO1, with 5wt% carbon black in it, needs a lower temperature for degradation in comparison to what was obtained in section 4.3. This results from the presence of carbon black in the film, which makes its color black. When LTO is used as only powder in the compound, the film color is white and cannot absorb the light as when carbon black is mixed with the compound. For LTO1, 190℃ for 7':30" results in complete degradation of PPC without any cracking on the surface.

Same reasoning can be used for LFP1 and LFP2, which are LFP compounds. They have carbon black in them, which makes their color darker and absorb more energy from the same radiation.

PPC degradation in these compounds completed after 5 min at 180℃, which is 10℃ lower than what was observed in section 4.3 for 20 vol% LFP compound.

In graphite containing final compounds, higher energy and therefore higher thermocouple temperature was needed for degradation. This is due to the dissipation of energy by graphite. Graphite is used as a heat sink which can dissipate energy to avoid very high temperatures on electronic devices [77] and it is the result of its layer structure. In the final compounds, graphite content is higher than in primary compounds. Compact layers of high content graphite make dissipation of energy more intense. Therefore, in comparison to section 4.3, instead of an isothermal degradation method, a ramp for increasing thermocouple temperature is used. In the previous section, when the thermocouple was kept at 200℃, sample temperature which was measured by FLIR camera reached 280℃. In this section, a higher thermocouple temperature is needed for reaching 280℃. For G1 and G2, temperature increased from 150℃ to 250℃. G3 sample temperature increased from 150℃ to 260℃. For G1 that has HNBR as binder, temperature of the sample on the surface went as high as 290℃. The lowest sample temperature was recorded for G4, which has the highest graphite content and energy dissipation was stronger. This compound also needed more time for degradation (8’:30”). For G1, G2 and G3, the only difference is in their matrix. It can be said that HNBR structure helped in reducing the amount of dissipated energy. For these three compounds, 6’:30” was needed for complete degradation of PPC.

Degradation condition of these compounds before using infrared heating lamps, as mentioned in a patent by Hutchinson [7], is being in an oven at 230℃ for at least 45 min. Using infrared heating lamps reduced time and energy for degradation of PPC in electrode compound significantly compared to conventional oven heating systems.

4.5 Scanning Electron Microscopy (SEM)

After complete degradation of PPC in the final compounds, SEM test were performed on them. To analyze samples with SEM, surface and cross-section images of films with the thickness of 100 microns and after degradation were taken. To calculate pore size and their density in each film, MIPAR software was used. The software highlights porous area, by choosing an appropriate threshold based on the pixel intensity, and gives an estimation for pore size and density. Figure 4-18 shows an example of how this software selects porous area. Then, by measuring the thickness of each feature, pore size will be calculated.

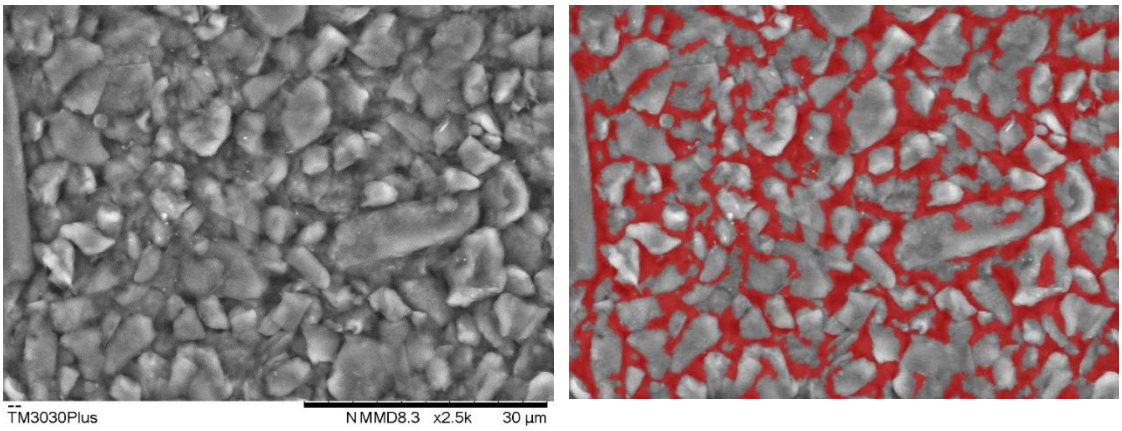

Figure 4-18. SEM micrograph of G1 film surface (left) and definition of porous area by MIPAR for calculating pore size and distribution (right)

On the right side of Figure 4-18, red area indicates porous area of the G1 sample. By this method, average pore size of this sample is 0.5 µm and 35% of the surface is the porous area fraction. This was done for all samples and the results are presented in Table 4-5. Figure 4-19 to Figure 4-24 show SEM micrograph of each sample for its surface and cross section.

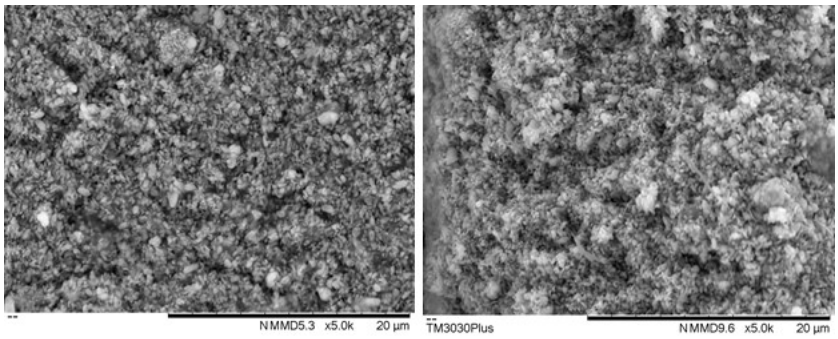

Figure 4-19. SEM micrograph of LFP1 surface (right) and cross section (left)

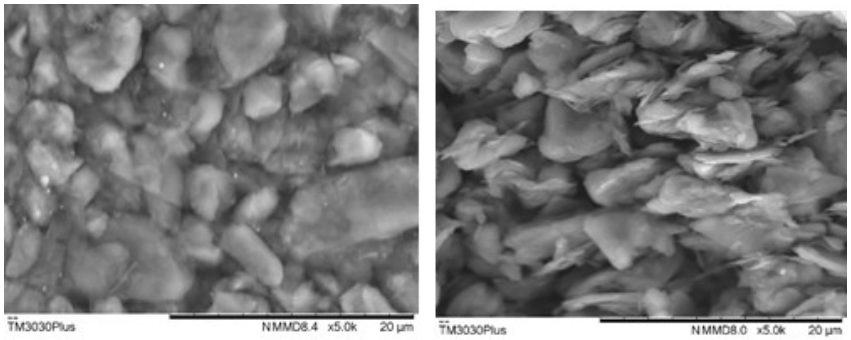

Figure 4-20. SEM micrograph of G1 (Graphite compound) surface (right) and cross section (left)

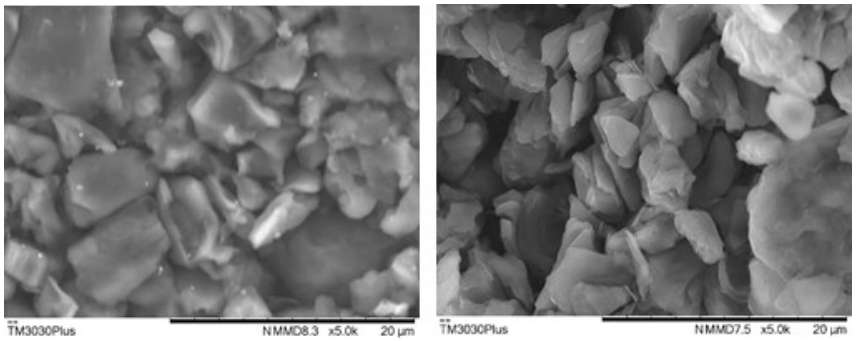

Figure 4-21. SEM micrograph of G2 (Graphite compound) surface (right) and cross section (left)

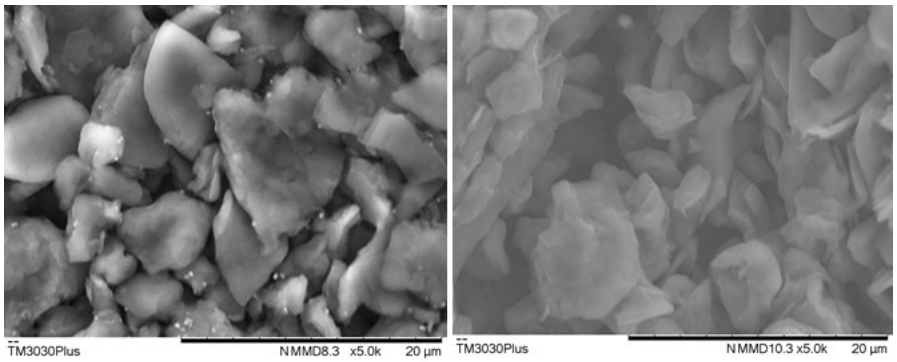

Figure 4-22. SEM micrograph of G3 (Graphite compound) surface (right) and cross section (left)

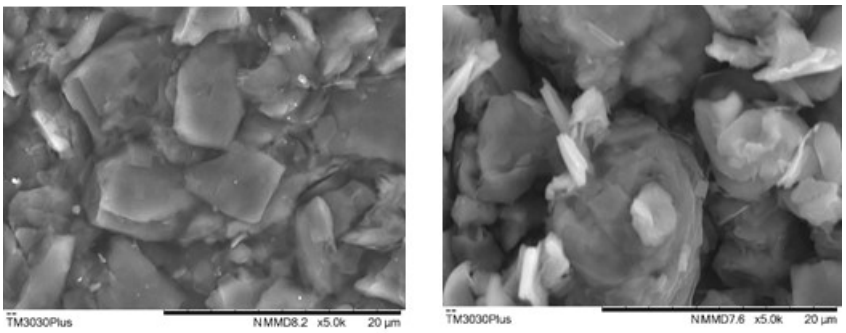

Figure 4-23. SEM micrograph of G4 (Graphite compound) surface (right) and cross section (left)

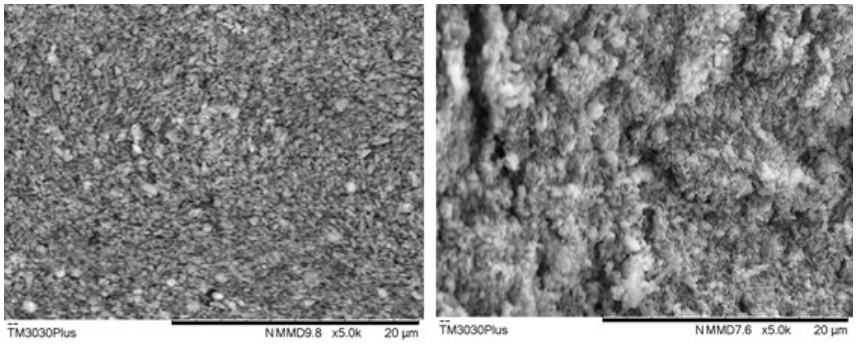

Figure 4-24. SEM micrograph of LFP2 surface (right) and cross section (left)

Graphite containing compounds are distinguishable by the big plate-shape graphite structure. It can be expected that bigger pore sizes will be related to the graphite compounds. Other active ingredients have much smaller powder size. In cross section image of all graphite compounds (G1, G2, G3 and G4), more flakes with perpendicular orientation to the surface are observed. In both surface and cross section of these samples, pores with different shapes and sizes are observable,

which is an indicator of non-uniform pore size in the samples. No preferential orientation is observed for LFP and LTO compounds.

The average pore size of each compound, pore size mode in the pore size distribution of each compound and total porous area on the surface and cross-section of each sample is calculated from the data which was obtained from MIPAR software and is presented in Table 4-5. These characteristics were calculated in 2 to 4 different locations and magnifications for each compound. Higher magnification (more than 5K) results in higher accuracy in pore size estimation and lower magnification results in better estimation for porous area density. Pore size distributions for all compound are presented in Figure 4-25 to Figure 4-31.

Table 4-5. Average pore size and porous area fraction of final compounds derived from SEM images

Code	Area studied	Average Pore size (µm)	Porous area fraction	Pore size mode (µm)
G1	Surface	0.6	34%	0.6
	Cross section	0.7	36%	0.65
G2	Surface	0.56	39%	0.75
	Cross section	0.6	37%	0.6
G3	Surface	0.7	35.50%	0.6
	Cross section	0.65	32%	0.6
G4	Surface	0.65	29.50%	0.6
	Cross section	0.7	32%	0.6
LFP2	Surface	0.25	40%	0.2
	Cross section	0.35	36%	0.2
LFP1	Surface	0.3	39%	0.25
	Cross section	0.35	42%	0.3
LTO 1	Surface	0.25	39%	0.2
	Cross section	0.35	41%	0.3

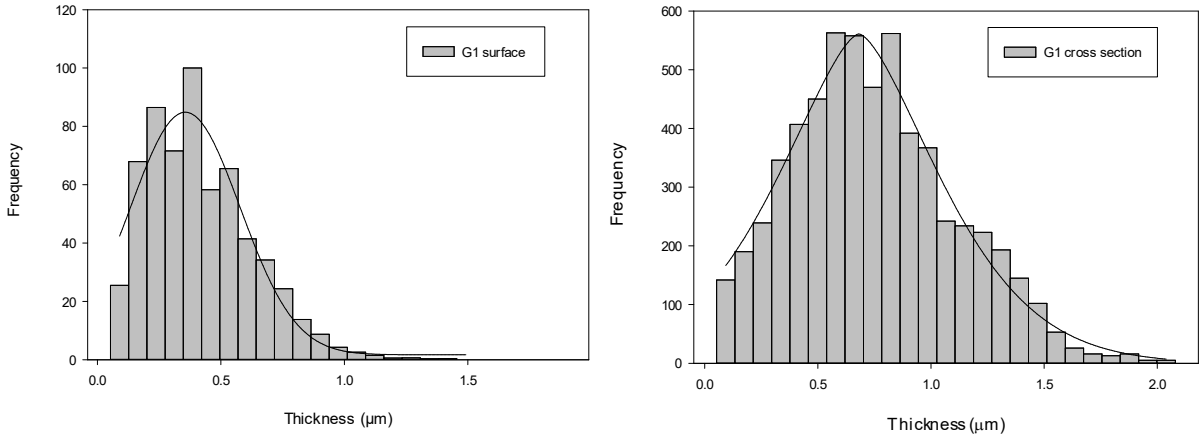

Figure 4-25. Pore size distribution of G1 measured by SEM. Surface (right) and cross section (left)

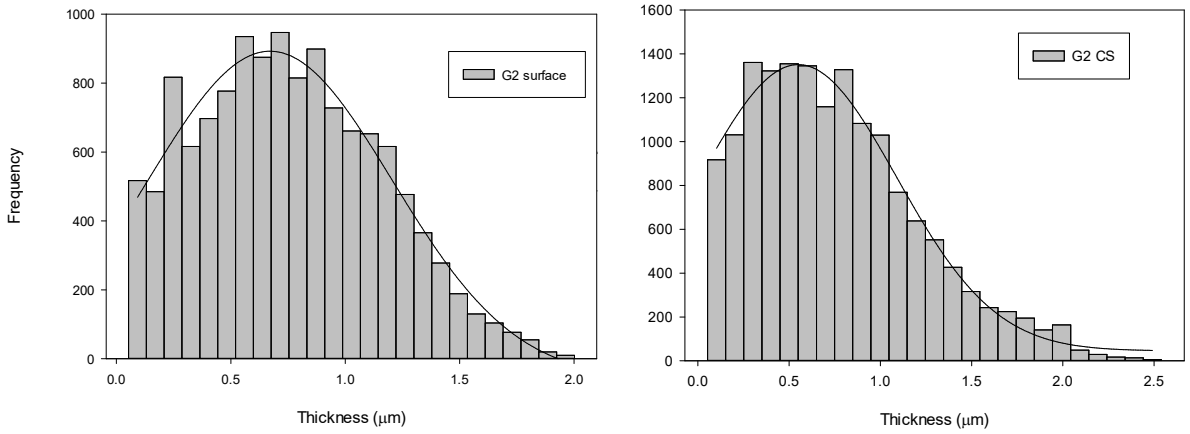

Figure 4-26. Pore size distribution of G2 measured by SEM. Surface (right) and cross section (left)

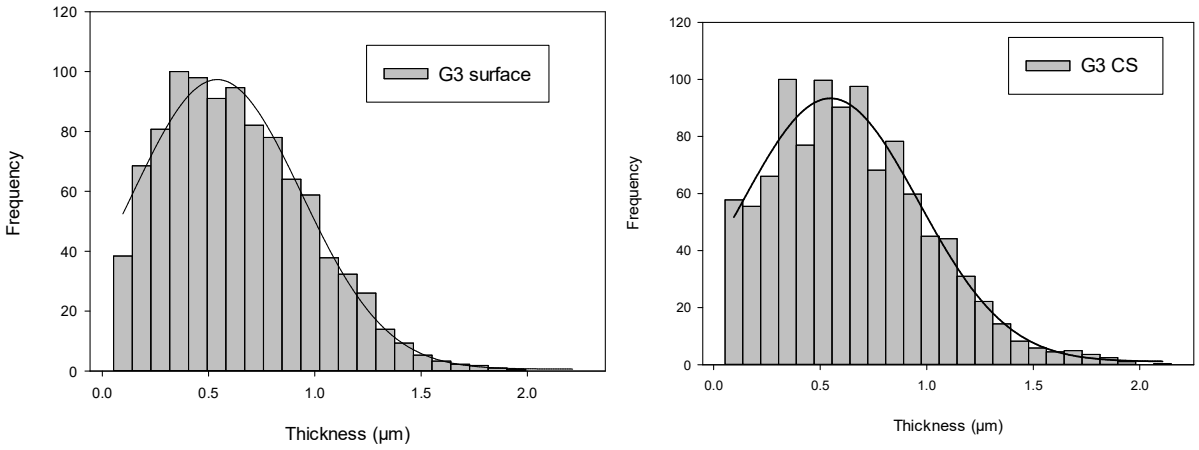

Figure 4-27. Pore size distribution of G3 measured by SEM. Surface (right) and cross section (left)

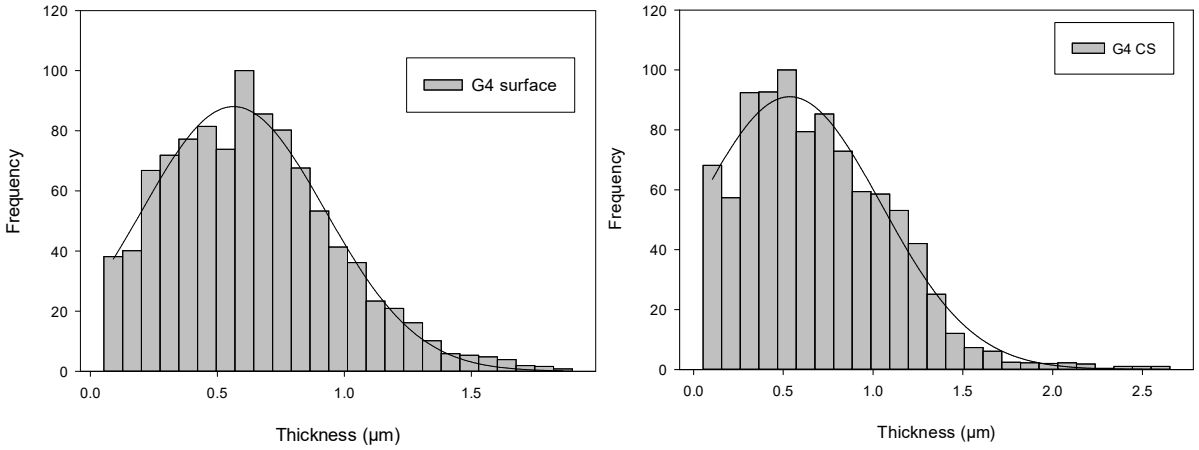

Figure 4-28. Pore size distribution of G4 measured by SEM. Surface (right) and cross section (left)

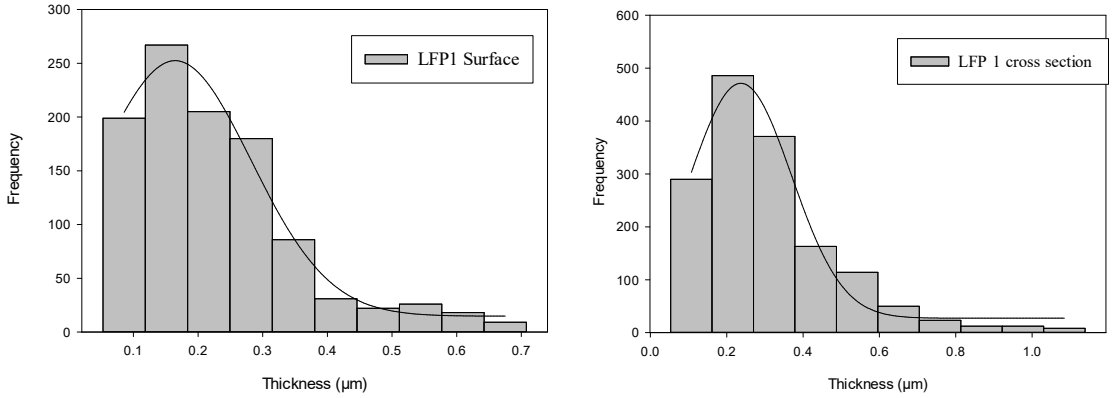

Figure 4-29. Pore size distribution of LFP1 measured by SEM. Surface (right) and cross section (left)

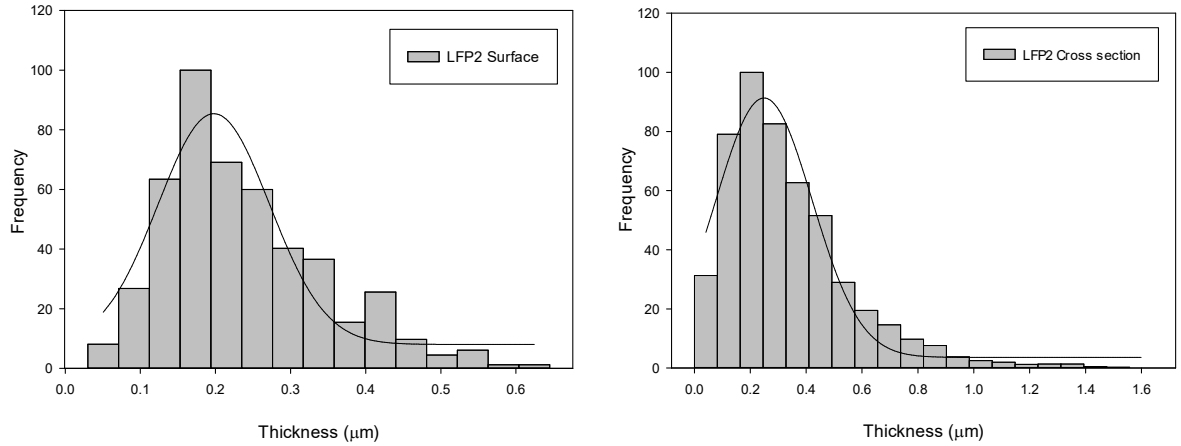

Figure 4-30. Pore size distribution of LFP2 measured by SEM. Surface (right) and cross section (left)

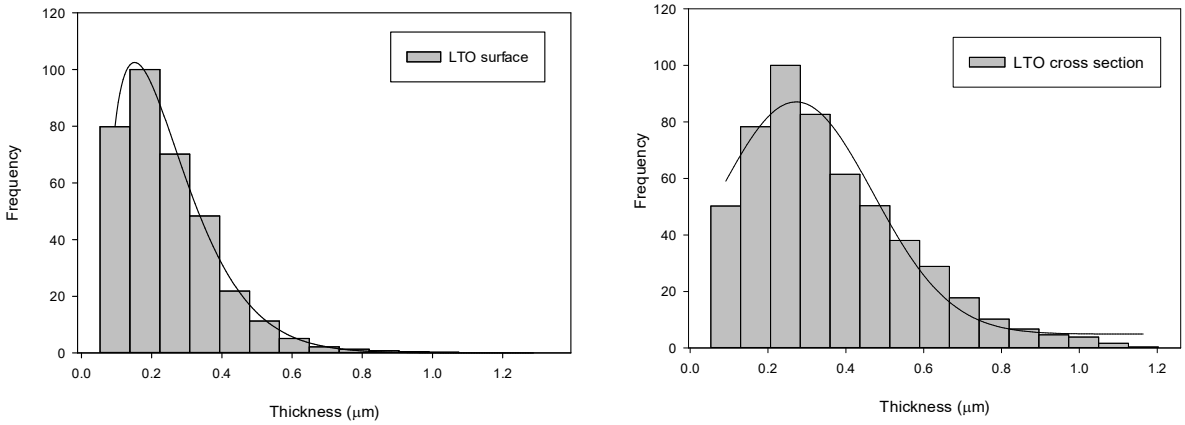

Figure 4-31. Pore size distribution of LTO measured by SEM. Surface (right) and cross section (left)

Based on these results, as expected before, graphite compounds have larger pore size. This is the result of flaky shaped particles in graphite with bigger particle size. There is a slight difference between pore size on the surface and cross section, which is negligible. Although in SEM micrographs a preferential orientation of graphite flakes perpendicular to the surface is observed, based on measurements, there is no significant difference between cross section and surface.

To check if the decomposition under infrared lamps in homogeneous through the electrode film, a 100 μm G1 film was put under infrared and the same ramp procedure for increasing temperature was taken. Instead of waiting for 6':30" for complete decomposition, the sample was taken out after 3 min. The cross-section of the half-decomposed sample was analyzed with SEM. The picture showed that the porosity is homogeneous through the cross-section but the total porosity is lower (24%) than the fully decomposed sample as expected.

4.6 Mercury Intrusion Porosimetry (MIP)

As mentioned before in chapter 2, MIP is an expensive test with environmental hazard. On the other hand, it is the most precise test for porosity measurement. Due to the problems associated with this test, is was only done on 2 graphite samples to evaluate the results obtained by SEM. G1 and G2, which have the same amount of active filler and sacrificial phase, with different binders, were put to test in MIP. Before testing, densities of these samples were measured by measuring the weight of the films and its volume (width*length*thickness). G1 density was 1.5 gr/cm^3 and G2 density was 1.2 gr/cm^3. Total porosity of each sample is calculated by

$$\emptyset = 1 - \frac{Apparent\ density}{bulk\ density}$$ Equation 4-7

Apparent density is defined by total mass of the sample divided by summation of apparent volume of the sample and volume of the pores. Bulk density in the density of the sample without taking pore density into consideration. Therefore, Equation 4-7 can be rearranged to the following equation:

$$\emptyset = \frac{Pore\ volume}{Total\ volume\ of\ the\ sample}$$ Equation 4-8

MIP test gives average pore size, pore size distribution and total pore volume. The following figures show the normalized pore size distribution of G1 and G2. The average pore size of G1 and G2 are both 1.1 μm, whereas the mode in their pore size distribution is 1.3 and 0.8 μm respectively.

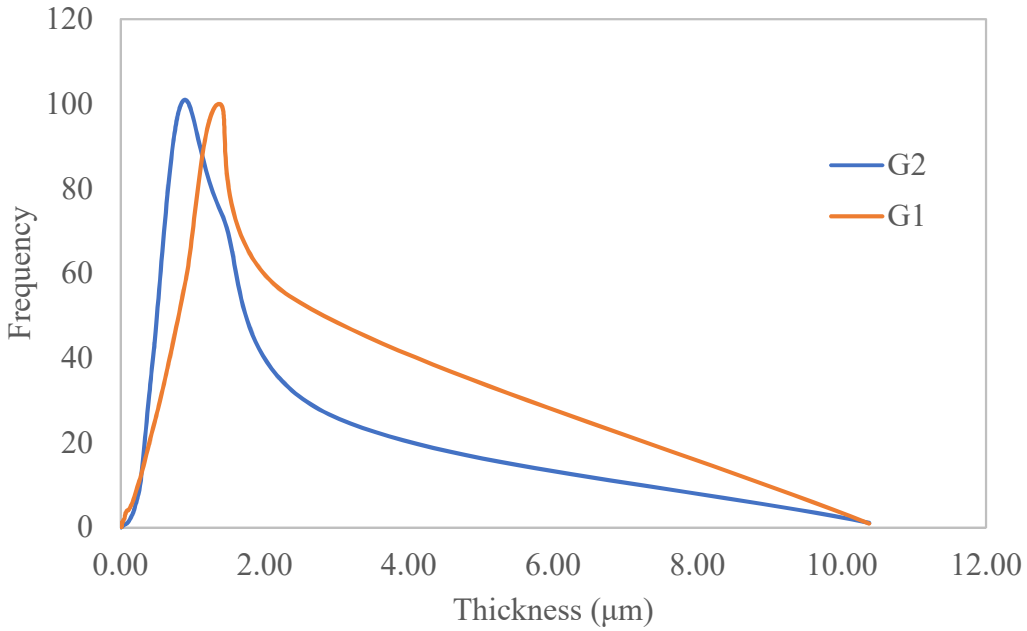

Figure 4-32. Pore size distribution of G1 and G2, measured by MIP

The following table shows the characteristics of each sample for porosity calculation.

Table 4-6. Graphite sample characteristics in MIP test

Sample Name	Weight (g)	Apparent density(gr/cm^3)	Apparent volume(cm^3)	Total pore volume measured by MIP(cm^3)
G1	0.2848	1.5	0.189	0.08
G2	0.4002	1.2	0.333	0.18

Based on these information, the total porosity of each sample is calculated as follows:

$$\Phi_{G1} = 39.4\%$$

$$\Phi_{G2} = 54\%$$

In comparison to SEM results, the total porosity and pore size measured by MIP is larger in both samples and they have higher total porosity. The underestimation of pore size and total porosity by SEM was mentioned in the literature review [57]. The undegraded samples of G1 and G2 had respectively 42 and 45 vol% of PPC. The final porosity of each sample should be identical to the volume fraction of PPC in each sample. The error in calculation of porosity in MIP might arise from the fact that, in MIP, the voids between particles are also filled with mercury and is reported in the result. Therefore, porosity of G2 is higher than what it was expected.

To confirm the total porosity of G1 and G2, pore volume of each sample was measured by using ethanol as a high wetting liquid to diffuse into the pores. Samples were immersed into the ethanol and after 30 min were removed from the liquid. The surface was wiped from liquid and the weight of sample before and after immersion was measured. With the assumption of not having any closed pores and calculating the volume of ethanol, pore volume can be obtained. Table 4-7 shows the calculation of pore volume in G1 and G2. Density of ethanol is 0.789 gr/cc.

Table 4-7. Porosity calculation by liquid saturation method

Sample Code	Sample density (gr/cc)	Sample weight before immersion (mg)	Sample volume before immersion (μL)	Sample weight after immersion (mg)	Ethanol weight (mg)	Ethanol volume (μL)	Total porosity
G1	1.4	8.7	6.2	10	2.1	2.7	43.5%
G2	1.2	6.6	5.5	8.8	2.2	2.8	51%

Calculated porosity of the samples from liquid saturation is close to the results of MIP. Although, this method is not accurate and is here to only have a comparison between different methods.

SEM, MIP and liquid saturation method results are compared in the following table.

Table 4-8. Summarized results of porosimetry

Sample code	Porosity by SEM (%)	Pore size average by SEM (μm)	Porosity by MIP (%)	Pore seize average by MIP(μm)	Porosity by liquid saturation (%)
G1	35	0.65	42	1.1	43.5
G2	38	0.6	54	1.1	45

Based on the final results presented in Table 4-8, while using SEM for porosity measurement, underestimation of the results by this technique should be considered. Liquid saturation method results give an estimation for the total porosity, but it cannot provide any information about the pore size. By the way, this method is the quickest and the easiest one when only total pore volume is needed.

CHAPTER 5 CONCLUSIONS

To lower degradation temperature of polypropylene carbonate, 3 catalysts (a photo acid generator, a thermal acid generator and a peroxide catalyst) were added to it. None of these catalysts were effective in decreasing decomposition temperature and, in some cases, even increased decomposition temperature. According to these results and the fact that the catalysts are expensive and might cause difficulties when mixed with other ingredients in the compound, they were not used in the electrode compounds.

First, active ingredients were hot mixed with the binder and sacrificial phase separately. TGA Results showed that graphite and carbon black increased the degradation temperature of PPC. On the other hand, LTO, CLTO and LFP decreased the degradation temperature of PPC.

Between 3 different infrared lamps, with different wavelength range, Carbon lamps increased the decomposition rate of PPC. The wavelength range of carbon lamps, that produce the highest level of energy, overlaps the peaks of energy absorption of PPC in UV-VIS-NIR tests. Time and temperature for degradation of each compound under infrared lamps were optimized and suggested. It was found that the compounds which contain graphite as active ingredient, need more time and higher temperature to decompose. Also, to avoid bubbling in graphite compounds, degradation cannot be done in isothermal condition and it should be increased in a ramp manner.

Porosity of final electrode compounds was studied using SEM, MIP and solvent saturation method. By comparing MIP and SEM results, it was concluded that porosity measurement by SEM imaging technique underestimates the pore size and the total porosity. Pore size of the compounds that contain graphite is larger than the compounds containing LFP or LTO. This was expected since graphite particles are much larger than LFP or LTO particles. Solvent saturation method could make a reasonable estimation for total porosity.

RECOMMENDATIONS

1. Photoacid generator and thermal acid generator could be added to the PPC in higher and lower weight fractions and studied.
2. The effect of PAG and TAG can be studied after being exposed to UV lamps. Specially in the case of PAG, it can be activated faster this way.
3. Catalysts could be added to the final compounds to study their effect in the presence of active ingredients.
4. Other types of catalysts could be examined for faster degradation of PPC.
5. Gas Pycnometry could be used as a more precise method for density and total porosity measurement.

REFERENCES

[1] W.-J. Zhang, "A review of the electrochemical performance of alloy anodes for lithium-ion batteries," *Journal of Power Sources,* vol. 196, no. 1, pp. 13-24, 2011.

[2] J. B. Goodenough and K.-S. Park, "The Li-ion rechargeable battery: a perspective," *Journal of the American Chemical Society,* vol. 135, no. 4, pp. 1167-1176, 2013.

[3] P. G. Bruce, B. Scrosati, and J. M. Tarascon, "Nanomaterials for rechargeable lithium batteries," *Angewandte Chemie International Edition,* vol. 47, no. 16, pp. 2930-2946, 2008.

[4] A. Vu, Y. Qian, and A. Stein, "Porous Electrode Materials for Lithium-Ion Batteries–How to Prepare Them and What Makes Them Special," *Advanced Energy Materials,* vol. 2, no. 9, pp. 1056-1085, 2012.

[5] J. B. Goodenough and Y. Kim, "Challenges for rechargeable Li batteries," *Chemistry of materials,* vol. 22, no. 3, pp. 587-603, 2009.

[6] D. Aurbach, M. D. Levi, E. Levi, and A. Schechter, "Failure and stabilization mechanisms of graphite electrodes," *The Journal of Physical Chemistry B,* vol. 101, no. 12, pp. 2195-2206, 1997.

[7] P. Sonntag, D. Ayme-Perrot, B. Dufour, A. PREBE, and N. Garois, "Method for preparing an electrode composition or a composition having magnetic properties, mixture and composition obtained by said method, and said electrode," ed: Google Patents, 2015.

[8] H. Lee, J. K. Yoo, J. H. Park, J. H. Kim, K. Kang, and Y. S. Jung, "A Stretchable Polymer–Carbon Nanotube Composite Electrode for Flexible Lithium-Ion Batteries: Porosity Engineering by Controlled Phase Separation," *Advanced Energy Materials,* vol. 2, no. 8, pp. 976-982, 2012.

[9] W. Bauer, D. Nötzel, V. Wenzel, and H. Nirschl, "Influence of dry mixing and distribution of conductive additives in cathodes for lithium ion batteries," *Journal of Power Sources,* vol. 288, no. Supplement C, pp. 359-367, 2015/08/15/ 2015.

[10] P. Sonntag, D. Ayme-Perrot, B. Dufour, A. Prebe, and N. Garois, "Process for preparing an electrode composition or composition with magnetic properties, mixture and composition obtained by means of said process and said electrode," ed: Google Patents, 2014.

[11] S. Oh, T. Fujiwara, Y. Kikuchi, and T. Yambe, "Method for manufacturing bonded magnet and method for manufacturing magnetic device having bonded magnet," ed: Google Patents, 2009.

[12] M. Yoshio, R. J. Brodd, and A. Kozawa, *Lithium-ion batteries*. Springer, 2009.

[13] B. Scrosati and J. Garche, "Lithium batteries: Status, prospects and future," *Journal of Power Sources,* vol. 195, no. 9, pp. 2419-2430, 2010.

[14] M. Winter and R. J. Brodd, "What are batteries, fuel cells, and supercapacitors?," ed: ACS Publications, 2004.

[15] Y. Wu, *Lithium-ion batteries: Fundamentals and Applications*. CRC Press, 2015.

[16] Y.-S. Park, E.-S. Oh, and S.-M. Lee, "Effect of polymeric binder type on the thermal stability and tolerance to roll-pressing of spherical natural graphite anodes for Li-ion batteries," *Journal of Power Sources,* vol. 248, pp. 1191-1196, 2014.

[17] T. J. Spencer and P. A. Kohl, "Decomposition of poly(propylene carbonate) with UV sensitive iodonium salts," *Polymer Degradation and Stability,* vol. 96, no. 4, pp. 686-702, 2011/04/01/ 2011.

[18] X. Zhou, F. Wang, Y. Zhu, and Z. Liu, "Graphene modified LiFePO 4 cathode materials for high power lithium ion batteries," *Journal of Materials Chemistry,* vol. 21, no. 10, pp. 3353-3358, 2011.

[19] K. Konstantinov *et al.*, "New approach for synthesis of carbon-mixed LiFePO 4 cathode materials," *Electrochimica acta,* vol. 50, no. 2, pp. 421-426, 2004.

[20] L. Qiu, Z. Shao, D. Wang, W. Wang, F. Wang, and J. Wang, "Enhanced electrochemical properties of LiFePO 4 (LFP) cathode using the carboxymethyl cellulose lithium (CMC-Li) as novel binder in lithium-ion battery," *Carbohydrate polymers,* vol. 111, pp. 588-591, 2014.

[21] J. Wang and X. Sun, "Understanding and recent development of carbon coating on LiFePO 4 cathode materials for lithium-ion batteries," *Energy & Environmental Science,* vol. 5, no. 1, pp. 5163-5185, 2012.

[22] H. Zhang, Y. Xu, C. Zhao, X. Yang, and Q. Jiang, "Effects of carbon coating and metal ions doping on low temperature electrochemical properties of LiFePO 4 cathode material," *Electrochimica Acta,* vol. 83, pp. 341-347, 2012.

[23] K.-F. Hsu, S.-Y. Tsay, and B.-J. Hwang, "Synthesis and characterization of nano-sized LiFePO 4 cathode materials prepared by a citric acid-based sol–gel route," *Journal of Materials Chemistry,* vol. 14, no. 17, pp. 2690-2695, 2004.

[24] X. Yuan, H. Liu, and J. Zhang, *Lithium-ion batteries: advanced materials and technologies*. CRC press, 2011.

[25] A. Izumi *et al.*, "Development of high capacity lithium-ion battery applying three-dimensionally patterned electrode," *Electrochimica Acta,* vol. 79, pp. 218-222, 2012.

[26] V. V. Viswanathan *et al.*, "Effect of entropy change of lithium intercalation in cathodes and anodes on Li-ion battery thermal management," *Journal of Power Sources,* vol. 195, no. 11, pp. 3720-3729, 2010.

[27] H.-G. Jung, N. Venugopal, B. Scrosati, and Y.-K. Sun, "A high energy and power density hybrid supercapacitor based on an advanced carbon-coated Li 4 Ti 5 O 12 electrode," *Journal of Power Sources,* vol. 221, pp. 266-271, 2013.

[28] H.-G. Jung, M. W. Jang, J. Hassoun, Y.-K. Sun, and B. Scrosati, "A high-rate long-life Li 4 Ti 5 O 12/Li [Ni 0.45 Co 0.1 Mn 1.45] O 4 lithium-ion battery," *Nature communications,* vol. 2, p. 516, 2011.

[29] D. Aurbach, E. Zinigrad, Y. Cohen, and H. Teller, "A short review of failure mechanisms of lithium metal and lithiated graphite anodes in liquid electrolyte solutions," *Solid state ionics,* vol. 148, no. 3, pp. 405-416, 2002.

[30] C. De las Casas and W. Li, "A review of application of carbon nanotubes for lithium ion battery anode material," *Journal of Power Sources,* vol. 208, pp. 74-85, 2012.

[31] L. J. Fu, K. Endo, K. Sekine, T. Takamura, Y. P. Wu, and H. Q. Wu, "Studies on capacity fading mechanism of graphite anode for Li-ion battery," *Journal of Power Sources,* vol. 162, no. 1, pp. 663-666, 2006/11/08/ 2006.

[32] D. Aurbach, H. Teller, M. Koltypin, and E. Levi, "On the behavior of different types of graphite anodes," *Journal of power sources,* vol. 119, pp. 2-7, 2003.

[33] M. Winter, J. O. Besenhard, M. E. Spahr, and P. Novák, "Insertion electrode materials for rechargeable lithium batteries," *Advanced materials,* vol. 10, no. 10, pp. 725-763, 1998.

[34] M. Obrovac and L. Christensen, "Structural changes in silicon anodes during lithium insertion/extraction," *Electrochemical and Solid-State Letters,* vol. 7, no. 5, pp. A93-A96, 2004.

[35] B. Gao *et al.*, "Enhanced saturation lithium composition in ball-milled single-walled carbon nanotubes," *Chemical Physics Letters,* vol. 327, no. 1, pp. 69-75, 2000.

[36] Z.-h. Yang and H.-q. Wu, "Electrochemical intercalation of lithium into fullerene soot," *Materials Letters,* vol. 50, no. 2, pp. 108-114, 2001.

[37] B. Gao *et al.*, "Electrochemical intercalation of single-walled carbon nanotubes with lithium," *Chemical Physics Letters,* vol. 307, no. 3, pp. 153-157, 1999.

[38] L. Huang, J.-S. Cai, Y. He, F.-S. Ke, and S.-G. Sun, "Structure and electrochemical performance of nanostructured Sn–Co alloy/carbon nanotube composites as anodes for lithium ion batteries," *Electrochemistry Communications,* vol. 11, no. 5, pp. 950-953, 2009.

[39] M. G. Cupta, P. J. Joseph, and P. A. Kohl, "Photoacid generators for catalytic decomposition of polycarbonate," *Journal of applied polymer science,* vol. 105, no. 5, pp. 2655-2662, 2007.

[40] O. Phillips, J. M. Schwartz, and P. A. Kohl, "Thermal decomposition of poly (propylene carbonate): End-capping, additives, and solvent effects," *Polymer Degradation and Stability,* vol. 125, pp. 129-139, 2016.

[41] C. A. Jones and J. M. DeSimone, "Critical Phase Polymerizations," *Encyclopedia of Polymer Science and Technology,* 2002.

[42] S. D. Thorat, P. J. Phillips, V. Semenov, and A. Gakh, "Physical properties of aliphatic polycarbonates made from CO2 and epoxides," *Journal of applied polymer science,* vol. 89, no. 5, pp. 1163-1176, 2003.

[43] L. Du, B. Qu, Y. Meng, and Q. Zhu, "Structural characterization and thermal and mechanical properties of poly (propylene carbonate)/MgAl-LDH exfoliation nanocomposite via solution intercalation," *Composites Science and Technology,* vol. 66, no. 7, pp. 913-918, 2006.

[44] L. Gao, M. Xiao, S. Wang, and Y. Meng, "Thermally stable poly (propylene carbonate) synthesized by copolymerizing with bulky naphthalene containing monomer," *Journal of applied polymer science,* vol. 108, no. 2, pp. 1037-1043, 2008.

[45] Q. Liu, Y. Zou, Y. Bei, G. Qi, and Y. Meng, "Mechanic properties and thermal degradation kinetics of terpolymer poly (propylene cyclohexene carbonate) s," *Materials Letters,* vol. 62, no. 17, pp. 3294-3296, 2008.

[46] H. Yan, W. R. Cannon, and D. J. Shanefield, "Thermal decomposition behaviour of poly(propylene carbonate)," *Ceramics International,* vol. 24, no. 6, pp. 433-439, 1998/01/01/ 1998.

[47] G. A. Luinstra, "Poly (propylene carbonate), old copolymers of propylene oxide and carbon dioxide with new interests: catalysis and material properties," *Polymer Reviews,* vol. 48, no. 1, pp. 192-219, 2008.

[48] G. A. Luinstra, G. R. Haas, F. Molnar, V. Bernhart, R. Eberhardt, and B. Rieger, "On the formation of aliphatic polycarbonates from epoxides with chromium (III) and aluminum (III) metal–salen complexes," *Chemistry-A European Journal,* vol. 11, no. 21, pp. 6298-6314, 2005.

[49] X. Li, S. Tjong, Y. Meng, and Q. Zhu, "Fabrication and properties of poly (propylene carbonate)/calcium carbonate composites," *Journal of Polymer Science Part B: Polymer Physics,* vol. 41, no. 15, pp. 1806-1813, 2003.

[50] X. Ma, P. R. Chang, J. Yu, and N. Wang, "Preparation and properties of biodegradable poly (propylene carbonate)/thermoplastic dried starch composites," *Carbohydrate Polymers,* vol. 71, no. 2, pp. 229-234, 2008.

[51] W. Ning, Z. Xingxiang, Y. Jiugao, and F. Jianming, "Partially miscible poly (lactic acid)-blend-poly (propylene carbonate) filled with carbon black as conductive polymer composite," *Polymer International,* vol. 57, no. 9, pp. 1027-1035, 2008.

[52] P. Song *et al.*, "Synthesis and properties of aliphatic polycarbonates derived from carbon dioxide, propylene oxide and maleic anhydride," *Journal of applied polymer science,* vol. 109, no. 6, pp. 4121-4129, 2008.

[53] T. Yu *et al.*, "Hydrogen-bonded thermostable liquid crystalline complex formed by biodegradable polymer and amphiphilic molecules," *Macromolecules,* vol. 41, no. 9, pp. 3175-3180, 2008.

[54] J. P. Jayachandran *et al.*, "Air-channel fabrication for microelectromechanical systems via sacrificial photosensitive polycarbonates," *Journal of Microelectromechanical Systems,* vol. 12, no. 2, pp. 147-159, 2003.

[55] K. L. Camera, B. Wenning, A. Lal, and C. K. Ober, "Transient materials from thermally-sensitive polycarbonates and polycarbonate nanocomposites," *Polymer,* vol. 101, pp. 59-66, 2016.

[56] V. Karageorgiou and D. Kaplan, "Porosity of 3D biomaterial scaffolds and osteogenesis," *Biomaterials,* vol. 26, no. 27, pp. 5474-5491, 2005/09/01/ 2005.

[57] L. M. Anovitz and D. R. Cole, "Characterization and analysis of porosity and pore structures," *Reviews in Mineralogy and geochemistry,* vol. 80, no. 1, pp. 61-164, 2015.

[58] A. Kaestner, E. Lehmann, and M. Stampanoni, "Imaging and image processing in porous media research," *Advances in Water Resources,* vol. 31, no. 9, pp. 1174-1187, 2008.

[59] M. Software. *User Manual*. Available: https://www.manula.com/manuals/mipar/user-manual/latest/en/topic/segmentation

[60] H. Giesche, "Mercury porosimetry: a general (practical) overview," *Particle & particle systems characterization,* vol. 23, no. 1, pp. 9-19, 2006.

[61] R. M. Lawrence, T. J. Mays, S. P. Rigby, P. Walker, and D. D'Ayala, "Effects of carbonation on the pore structure of non-hydraulic lime mortars," *Cement and concrete research,* vol. 37, no. 7, pp. 1059-1069, 2007.

[62] Y. Hu, D. W. Grainger, S. R. Winn, and J. O. Hollinger, "Fabrication of poly (α-hydroxy acid) foam scaffolds using multiple solvent systems," *Journal of Biomedical Materials Research Part A,* vol. 59, no. 3, pp. 563-572, 2002.

[63] C. Waters, M. Salih, and S. Ajinola, "Porosity comparative analysis of porous copper and OOF modelling," *Journal of Porous Materials,* journal article vol. 22, no. 4, pp. 989-995, August 01 2015.

[64] J. D. Menczel and R. B. Prime, *Thermal analysis of polymers: fundamentals and applications*. John Wiley & Sons, 2014.

[65] H. Co. Available: http://www.bumbas.ro/fisiere/1978__458.pdf

[66] M. Lawrence and Y. Jiang, "Porosity, Pore Size Distribution, Micro-structure," in *Bio-aggregates Based Building Materials*: Springer, 2017, pp. 39-71.

[67] D. A. Jerram and A. J. R. Kent, "An overview of modern trends in petrography: Textural and microanalysis of igneous rocks," *Journal of Volcanology and Geothermal Research,* vol. 154, no. 1, pp. vii-ix, 2006/06/01/ 2006.

[68] S. h. Kim and C. C. Chu, "Pore structure analysis of swollen dextran-methacrylate hydrogels by SEM and mercury intrusion porosimetry," *Journal of Biomedical Materials Research Part A,* vol. 53, no. 3, pp. 258-266, 2000.

[69] B. Mikijelj, J. ARANA VARELA, and O. Whittemore, "Equivalence of surface areas determined by nitrogen adsorption and by mercury porosimetry," *American Ceramic Society Bulletin,* vol. 70, no. 5, pp. 829-831, 1991.

[70] X. H. Li, Y. Z. Meng, Q. Zhu, and S. C. Tjong, "Thermal decomposition characteristics of poly(propylene carbonate) using TG/IR and Py-GC/MS techniques," *Polymer Degradation and Stability,* vol. 81, no. 1, pp. 157-165, 2003/01/01/ 2003.

[71] C. Puglisi, F. Samperi, S. Carroccio, and G. Montaudo, "MALDI− TOF Investigation of Polymer Degradation. Pyrolysis of Poly (bisphenol A carbonate)," *Macromolecules,* vol. 32, no. 26, pp. 8821-8828, 1999.

[72] B. N. Jang and C. A. Wilkie, "The thermal degradation of bisphenol A polycarbonate in air," *Thermochimica acta,* vol. 426, no. 1-2, pp. 73-84, 2005.

[73] W. Jiang and S. C. Tjong, "Thermal stability of polycarbonate composites reinforced with potassium titanate whiskers: effect of coupling agent addition," *Polymer Degradation and Stability,* vol. 66, no. 2, pp. 241-246, 1999/11/01/ 1999.

[74] S. Tjong and Y. Meng, "Mechanical and thermal properties of polycarbonate composites reinforced with potassium titanate whiskers," *Journal of applied polymer science,* vol. 72, no. 4, pp. 501-508, 1999.

[75] J. Bian, X. Wei, S. Gong, H. Zhang, and Z. Guan, "Improving the thermal and mechanical properties of poly (propylene carbonate) by incorporating functionalized graphite oxide," *Journal of Applied Polymer Science,* vol. 123, no. 5, pp. 2743-2752, 2012.

[76] M. Aden, A. Roesner, and A. Olowinsky, "Optical characterization of polycarbonate: Influence of additives on optical properties," *Journal of Polymer Science Part B: Polymer Physics,* vol. 48, no. 4, pp. 451-455, 2010.

[77] J. Norley, J.-W. Tzeng, and J. Klug, "Graphite-based heat sink," ed: Google Patents, 2003.